

Tennessee State University

## Digital Scholarship @ Tennessee State University

---

Information Systems and Engineering  
Management Research Publications

Center of Excellence in Information Systems  
and Engineering Management

---

9-8-2017

### The Quadruple-lined, Doubly Eclipsing System V482 Persei

Guillermo Torres

*Harvard-Smithsonian Center for Astrophysics*

Claud H. Sandberg Lacy

*University of Arkansas, Fayetteville*

Francis C. Fekel

*Tennessee State University*

Marek Wolf

*Charles University in Prague*

Matthew W. Muterspaugh

*Tennessee State University*

Follow this and additional works at: <https://digitalscholarship.tnstate.edu/coe-research>



Part of the [Stars, Interstellar Medium and the Galaxy Commons](#)

---




#### Recommended Citation

Guillermo Torres et al 2017 ApJ 846 115

This Article is brought to you for free and open access by the Center of Excellence in Information Systems and Engineering Management at Digital Scholarship @ Tennessee State University. It has been accepted for inclusion in Information Systems and Engineering Management Research Publications by an authorized administrator of Digital Scholarship @ Tennessee State University. For more information, please contact [XGE@Tnstate.edu](mailto:XGE@Tnstate.edu).



# The Quadruple-lined, Doubly Eclipsing System V482 Persei

Guillermo Torres<sup>1</sup> , Claud H. Sandberg Lacy<sup>2</sup> , Francis C. Fekel<sup>3</sup> , Marek Wolf<sup>4</sup>, and Matthew W. Muterspaugh<sup>3,5</sup>

<sup>1</sup>Harvard-Smithsonian Center for Astrophysics, 60 Garden Street, Cambridge, MA 02138, USA; [gtorres@cfa.harvard.edu](mailto:gtorres@cfa.harvard.edu)

<sup>2</sup>Physics Department, University of Arkansas, Fayetteville, AR 72701, USA

<sup>3</sup>Center of Excellence in Information Systems, Tennessee State University, Nashville, TN 37209, USA

<sup>4</sup>Astronomical Institute, Faculty of Mathematics and Physics, Charles University in Prague, 180 00 Praha 8, Czech Republic

<sup>5</sup>College of Life and Physical Sciences, Tennessee State University, Nashville, TN 37209, USA

Received 2017 June 21; revised 2017 August 1; accepted 2017 August 11; published 2017 September 8

## Abstract

We report spectroscopic and differential photometric observations of the A-type system V482 Per, which reveal it to be a rare hierarchical quadruple system containing two eclipsing binaries. One binary has the previously known orbital period of 2.4 days and a circular orbit, and the other a period of 6 days, a slightly eccentric orbit ( $e = 0.11$ ), and shallow eclipses only 2.3% deep. The two binaries revolve around their common center of mass in a highly elongated orbit ( $e = 0.85$ ) with a period of 16.67 yr. Radial velocities are measured for all components from our quadruple-lined spectra and are combined with the light curves and measurements of times of minimum light for the 2.4 day binary to solve for the elements of the inner and outer orbits simultaneously. The line-of-sight inclination angles of the three orbits are similar, suggesting they may be close to coplanar. The available observations appear to indicate that the 6 day binary experiences significant retrograde apsidal motion in the amount of about 60 deg per century. We derive absolute masses for the four stars good to better than 1.5%, along with radii with formal errors of 1.1% and 3.5% for the 2.4 day binary and  $\sim 9\%$  for the 6 day binary. A comparison of these and other physical properties with current stellar evolution models gives excellent agreement for a metallicity of  $[\text{Fe}/\text{H}] = -0.15$  and an age of 360 Myr.

*Key words:* binaries: eclipsing – stars: evolution – stars: fundamental parameters – stars: individual (V482 Per) – techniques: photometric – techniques: radial velocities

*Supporting material:* machine-readable tables

## 1. Introduction

The photometric variability of V482 Persei (alternate designations BD+47 961, TYC 3332–314–1;  $V = 10.25$ ,  $P = 2.44$  days) was discovered photographically by Hoffmeister (1966) at the Sonneberg Observatory on the basis of a single instance of a drop in brightness. The orbital period of 2.44 days was determined later by Harvig & Leis (1981), also photographically. The first photoelectric light curves ( $BV$ ) were published by Agerer & Lichtenknecker (1991), along with several times of minimum light. Continued recording of the times of eclipse by many authors eventually led to the discovery of the light-travel time effect (LTTE; Wolf et al. 2004), implying the presence of a third object in the system with a very eccentric ( $e \approx 0.82$ ) and long-period orbit ( $P \approx 16.8$  yr). Similar parameters for the third body were reported by Ogłóza et al. (2012). Popper (1996) remarked on an apparent discrepancy between the spectral type implied by the Agerer & Lichtenknecker (1991) observations and the weakness of the sodium D lines. He reported a type of F2. However, the most commonly seen classification of the star in the literature is A0 (e.g., Heckmann 1975), although other sources list the object as either A2 (Luo et al. 2016) or F6 (Pickles & Depagne 2010). More recently, Baştürk et al. (2015) published the first determination of the absolute properties of the V482 Per components based on new  $BVRI$  light curves and spectroscopic observations.

We placed V482 Per on our own photometric and spectroscopic observing program in 2001, also with the goal of deriving accurate physical properties for the stars. These observations reveal that the object is in reality a hierarchical quadruple system. Our spectra show four sets of lines

corresponding to the components of two binaries, with the brighter one having the reported period of 2.4 days and the other, a period of 6 days. Furthermore, this second binary is also eclipsing (although the eclipses are very shallow), and both systems orbit a common center of mass with the 16 year period inferred earlier from the LTTE. Such quadruple, doubly eclipsing systems are relatively rare, though several have been discovered in recent years based on the high-precision and nearly uninterrupted observations collected between 2009 and 2013 by NASA's *Kepler* spacecraft, as well as from ground-based surveys (see, e.g., Pawlak et al. 2013; Koo et al. 2014; Lohr et al. 2015).

Because V482 Per has a more complicated nature than it was thought to have at the time of the analysis by Baştürk et al. (2015), and because of the limited spectroscopic material these authors had at their disposal that did not allow them to resolve the four components, the properties they derived for the stars in the 2.4 day binary are incorrect. The motivation for this paper is thus to perform a complete and independent analysis of our observations with the new knowledge about the configuration of the system, to determine the physical properties of all four stars, and to compare them against stellar evolution models.

We begin in Section 2 by describing our spectroscopic and photometric observations, as well as the available times of minimum light for the 2.4 day binary. Our analysis of these data is presented in Section 3, where we solve for the orbits of the inner binaries and the outer orbit simultaneously. The physical properties we determine for the four stars are reported in Section 4, and a comparison with stellar evolution models is found in Section 5. We conclude with a discussion of the results in Section 6.

**Table 1**

Differential V-band Observations of V482 Per from the URSA WebScope

HJD-2,400,000	$\Delta V$ (mag)
52250.75606	0.019
52250.75697	0.023
52250.75789	0.029
52250.75879	0.020
52250.75971	0.031

(This table is available in its entirety in machine-readable form.)

## 2. Observations

### 2.1. Differential Photometry

Differential photometry of V482 Per was obtained by measuring images collected with two different robotic telescopes: the URSA WebScope at the University of Arkansas at Fayetteville, AR (Lacy et al. 2005), and the NFO WebScope near Silver City, NM (Grauer et al. 2008). The URSA WebScope consists of a 10 inch Meade LX 200 SCT with an SBIG ST8 CCD camera, housed in a Technical Innovations RoboDome on top of Kimpel Hall on campus. The NFO WebScope is a modified Group 128 24 inch Cassegrain telescope with a CCD camera in a roll-off enclosure. All observations were made through a Bessel V filter consisting of 2.0 mm of GG495 and 3.0 mm of BG39. Observations were made between 2001 December and 2016 January, and are presented in Tables 1 and 2. Two comparison stars were measured near the variable star (which has  $V = 10.25$ , SpT A0): TYC 3332-0388-1 ( $V = 10.22$ , SpT A5) and TYC 3332-0146-1 ( $V = 11.33$ ). A total of 13,000 frames of V482 Per were gathered with the URSA telescope, and 14,072 with the NFO WebScope. All images were measured with an application (*Measure*) written by author Lacy. The standard deviations of the differences in magnitudes between the two comparison stars were 0.012 mag for the URSA measurements and 0.015 mag for those from the NFO.

### 2.2. Spectroscopy

V482 Per was monitored spectroscopically with two different instruments. We observed it between 2009 November and 2017 February at the Harvard-Smithsonian Center for Astrophysics (CfA) with the Tillinghast Reflector Echelle Spectrograph (TRES; Szentgyorgyi & Fűrész 2007; Fűrész 2008), a fiber-fed, bench-mounted instrument on the 1.5 m Tillinghast reflector at the Fred L. Whipple Observatory (Mount Hopkins, AZ). The wavelength coverage is approximately 3900–9100 Å in 51 orders, with a resolving power of  $R \approx 44,000$ . For the radial-velocity measurements described below, we used a single order centered on the Mg I b triplet at 5188 Å, which yields the best results. A total of 46 spectra were gathered with typical signal-to-noise ratios between 30 and 100 per resolution element of  $6.8 \text{ km s}^{-1}$ . Wavelength calibrations were based on exposures of a thorium-argon lamp taken before and after each science frame, and radial-velocity standards were observed each night although they were not used because of the high stability of the spectrograph ( $\sim 20 \text{ m s}^{-1}$ , much better than required for this work). Reductions were performed with a custom pipeline.

From 2011 November through 2017 April, we additionally acquired 37 useful spectra of V482 Per with the Tennessee State

**Table 2**

Differential V-band Observations of V482 Per from the NFO WebScope

HJD-2,400,000	$\Delta V$ (mag)
53405.79764	0.555
53405.80017	0.547
53405.80271	0.546
53405.80519	0.542
53405.80773	0.538

(This table is available in its entirety in machine-readable form.)

University 2 m Automatic Spectroscopic Telescope (AST) and a fiber-fed echelle spectrograph (Eaton & Williamson 2007) at the Fairborn Observatory in southeast Arizona. The detector for these observations was a Fairchild 486 CCD, having a  $4096 \times 4096$  array of  $15 \mu\text{m}$  pixels. Although the spectrograms have 48 orders ranging from 3800 to 8260 Å, we used only the orders that cover the wavelength region from 4920 to 7100 Å. Because of the faintness of V482 Per and the moderate rotation of its components, we made our observations with a fiber that produced a spectral resolution of 0.4 Å, corresponding to a resolving power of 15,000 at 6000 Å. Our spectra have typical signal-to-noise ratios of 30–40 at this wavelength. More information about the AST facility can be found in the paper of Fekel et al. (2013).

Radial-velocity determinations from the TRES spectra proceeded as follows. Based on the expectation that we would see two sets of relatively broad lines corresponding to the components of the 2.4 day binary (binary “A”), initial determinations of the radial velocities were made with the two-dimensional cross-correlation technique TODCOR (Zucker & Mazeh 1994). It soon became clear that there were two additional sets of lines that were much sharper and did not phase up with the ephemeris for the 2.4 day binary (see Figure 1). They were eventually found to correspond to the primary and secondary of a 6 day binary (binary “B”). The final velocities for the four stars were then measured by extending TODCOR to four dimensions (QUADCOR; Torres et al. 2007). Templates (one for each star) were taken from a large library of synthetic spectra based on PHOENIX model atmospheres (Husser et al. 2013). The two main parameters of these templates, the effective temperature ( $T_{\text{eff}}$ ) and rotational velocity ( $v \sin i$ , when seen in projection), were determined by running extensive grids of cross-correlations over wide ranges seeking the best match to our spectra as measured by the average correlation coefficient. For an analogous methodology applied to the case of only two stars, see Torres et al. (2002). In this way we determined optimal temperatures of 10,600 K and 9600 K for the components of the 2.4 day binary, referred to in the following as stars Aa (the more massive one) and Ab. Estimated uncertainties are 200 K. For each star in the 6 day binary (Ba and Bb, with Ba being marginally more massive; see Section 4), we obtained 7600 K and larger uncertainties of 300 K due to their faintness. These temperatures correspond to spectral types of approximately B9 and A0 for the 2.4 day binary, and A6 for the stars in the 6 day binary (Gray 1992). The  $v \sin i$  values of stars Aa and Ab were determined from this procedure to be 60 and 40  $\text{km s}^{-1}$ , with uncertainties of 5  $\text{km s}^{-1}$ , and for Ba and Bb we measured  $12 \pm 2 \text{ km s}^{-1}$ . Surface gravities,  $\log g$ , were held at values of 4.0 for stars Aa and Ab, and 4.5 for Ba and Bb, close to the final values from our analysis. Solar metallicity was adopted

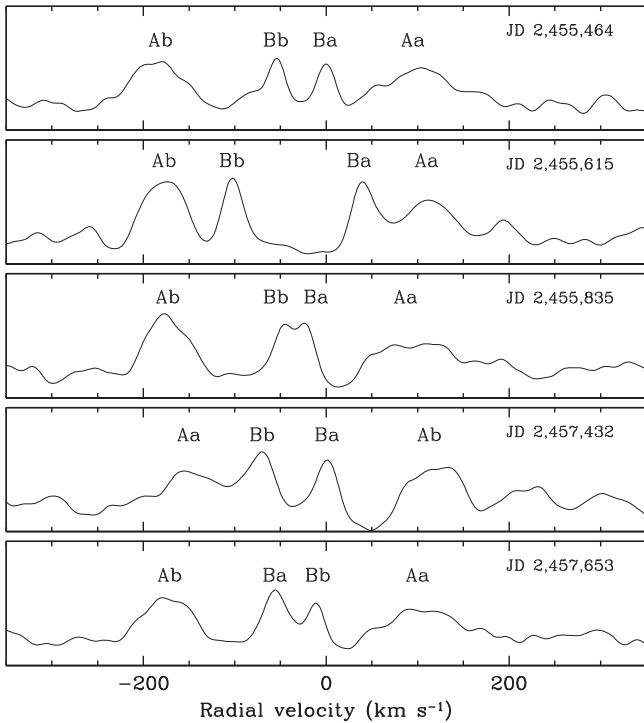


**Figure 1.** Examples of one-dimensional cross-correlation functions for V482 Per showing peaks corresponding to the lines of the four components, as labeled. The Julian dates are shown in each panel.

throughout, and modest changes in composition ( $\pm 0.5$  dex in  $[\text{Fe}/\text{H}]$ ) have a negligible effect on the measurements. The final TRES velocities in the heliocentric frame are listed in Table 3 along with their individual uncertainties, which have been adjusted to match the scatter from a preliminary joint orbital solution for the quadruple system that used the velocities of all four stars and the eclipse timings for binary A (see next section). The uncertainties average 3.3, 2.6, 1.3, and 1.3  $\text{km s}^{-1}$  for stars Aa, Ab, Ba, and Bb, respectively. The complicated nature of the spectra makes the flux ratios among the stars difficult to measure. Our estimates with QUADCOR yield  $\ell_{\text{Ab}}/\ell_{\text{Aa}} = 0.54 \pm 0.04$ ,  $\ell_{\text{Ba}}/\ell_{\text{Aa}} = 0.091 \pm 0.004$ , and  $\ell_{\text{Bb}}/\ell_{\text{Aa}} = 0.091 \pm 0.004$ , and a flux ratio within the 6 day binary of  $\ell_{\text{Bb}}/\ell_{\text{Ba}} = 1.01 \pm 0.06$ , all at the mean wavelength of our observations, 5188 Å.

Our AST spectra of V482 Per also clearly show four sets of lines, and so, line blending often occurs. In addition, the average depth of the lines is only about 1%–2%, and the lines of the 2.4 day binary have very significant rotational broadening. These factors contribute to the difficulty in measuring the radial velocities of the stars using the procedures applied to these spectra.

Fekel et al. (2009) presented a general explanation of the velocity measurement of the Fairborn echelle spectra. For the 6 day binary, we used our solar-type star line list to measure velocities because the lines of the 2.4 day binary are much less visible, and therefore cause significantly fewer blending problems. In addition, the solar line list has more than four times as many lines as the A star line list, so using that list improves the precision of the averaged velocities. To measure velocities of the 2.4 day binary, we used our A star line list, which consists mostly of lines of ionized elements. With that list, the features of all four stars are visible, and the average line depth of the four components is similar.

Our velocities were determined by fitting the individual lines with rotational broadening functions (Lacy & Fekel 2011), and we allowed both the depth and width of the line fits to vary. In the case of blended features, we fit both components of the blend simultaneously. A few velocities of the 6 day binary components were measured with the A star line list, and those velocities were found to be consistent with the ones measured with the solar-type star line list. In the end, we obtained 20 pairs of measurements for the 2.4 day binary and 32 pairs for the 6 day binary.

Our unpublished measurements of several IAU solar-type velocity standards show that these Fairborn Observatory velocities have a zero-point offset of  $-0.6 \text{ km s}^{-1}$  when compared to the results of Scarfe (2010). Thus, we have added  $0.6 \text{ km s}^{-1}$  to each velocity. Our useful Fairborn observations and the measured heliocentric velocities are given in Table 4. Typical uncertainties were estimated to be 5.4, 3.9, 1.3, and  $1.6 \text{ km s}^{-1}$  for stars Aa, Ab, Ba, and Bb, respectively, based on the scatter from the preliminary orbital solution mentioned earlier (see also Section 2.3).

Rotational broadening fits of the lines in our spectra that have the highest signal-to-noise ratios result in  $v \sin i$  values of  $59 \pm 5 \text{ km s}^{-1}$  and  $39 \pm 3 \text{ km s}^{-1}$  for the primary and secondary of the 2.4 day binary, respectively. For the 6 day binary components, we determine  $v \sin i$  values of  $11 \pm 2 \text{ km s}^{-1}$  and  $13 \pm 2 \text{ km s}^{-1}$  for stars Ba and Bb, respectively.

From the best Fairborn spectra, the average line equivalent width ratio of the components in the 6 day orbit is  $0.97 \pm 0.07$ , which should be indicative of the true light ratio  $\ell_{\text{Bb}}/\ell_{\text{Ba}}$  at all wavelengths as their effective temperatures are essentially the same. This measurement is consistent with our estimate from the CfA spectra.

### 2.3. Times of Minimum Light

Numerous times of minimum light have been recorded for the 2.4 day binary since its discovery. The few photographic estimates reported by Hoffmeister (1966) and Harvig & Leis (1981) are too poor to be useful for the present work. The other, more recent determinations are collected in Table 5 along with their reported uncertainties, where available. A total of 78 correspond to eclipses of star Aa, and 36 to those of Ab. They span 27.5 years, or about 1.6 cycles of the outer 16 year orbit between the A and B binaries.

Experience indicates that published uncertainties for this type of observation are not always accurate and are often underestimated. To test this, we carried out a solution for the outer orbit that used the times of minimum along with the radial velocities described earlier, modeling the third-body effect on the timings with the classical formalism by Irwin (1952, 1959). Based on the residuals from this fit, we established that the primary and secondary timing errors require scale factors of about 2.8 and 4.5 in order to obtain reduced  $\chi^2$  values near unity. Similarly, for measurements with no published errors, we found average uncertainties of 0.0027 days and 0.0010 days to be suitable for the primary and secondary timings, respectively. We adjusted the published errors accordingly, and adopted them for our analysis in Section 3.2. The same procedure was used to adjust the uncertainties for the radial velocities, as mentioned before, arriving at the values reported in Tables 3 and 4.



**Table 3**  
Heliocentric Radial-velocity Measurements of V482 Per from CfA

HJD (2,400,000+)	$RV_{Aa}$ ( $\text{km s}^{-1}$ )	$\sigma_{Aa}$ ( $\text{km s}^{-1}$ )	$RV_{Ab}$ ( $\text{km s}^{-1}$ )	$\sigma_{Ab}$ ( $\text{km s}^{-1}$ )	$RV_{Ba}$ ( $\text{km s}^{-1}$ )	$\sigma_{Ba}$ ( $\text{km s}^{-1}$ )	$RV_{Bb}$ ( $\text{km s}^{-1}$ )	$\sigma_{Bb}$ ( $\text{km s}^{-1}$ )	Phase Aa+Ab	Phase Ba+Bb
55143.8088	44.13	6.03	-162.22	4.63	-89.18	2.33	82.77	2.28	0.8500	0.1521
55144.8750	-153.37	7.18	99.24	5.52	-67.54	2.77	60.70	2.72	0.2858	0.3297
55171.7254	-167.97	5.61	100.16	4.31	66.70	2.17	-67.21	2.12	0.2604	0.8032
55192.7260	41.56	3.63	-176.48	2.79	-68.08	1.40	76.58	1.38	0.8440	0.3020
55199.7654	50.39	3.63	-200.03	2.79	24.48	1.40	-10.75	1.37	0.7213	0.4748
55227.7623	-155.56	3.79	70.51	2.91	-69.42	1.47	94.66	1.43	0.1648	0.1391
55464.0061	82.97	2.83	-180.60	2.18	-1.12	1.10	-54.90	1.07	0.7235	0.4997
55486.0085	72.73	3.67	-172.04	2.82	-115.84	1.42	60.88	1.39	0.7160	0.1658
55527.7138	90.56	3.71	-172.97	2.85	-102.76	1.43	40.82	1.40	0.7612	0.1149
55615.7548	88.54	1.72	-176.94	1.32	36.17	0.66	-102.89	0.65	0.7439	0.7846
55647.6127	81.97	3.42	-172.67	2.63	-93.14	1.32	25.58	1.30	0.7643	0.0929
55835.9381	87.20	2.38	-172.49	1.83	-22.29	0.92	-48.34	0.90	0.7332	0.4726
55846.9420	-140.60	1.82	121.07	1.40	-109.52	0.70	39.55	0.69	0.2305	0.3061
55851.9695	-135.74	4.56	117.66	3.50	-118.82	1.76	50.38	1.73	0.2852	0.1438
55879.9608	93.57	5.35	-174.91	4.11	32.57	2.07	-101.47	2.02	0.7253	0.8079
55882.9200	18.74	2.54	-87.11	1.96	-109.37	0.98	42.15	0.96	0.9347	0.3009
55883.9049	-127.93	1.96	99.27	1.50	-24.71	0.76	-45.75	0.74	0.3372	0.4650
55884.9629	88.13	4.12	-180.62	3.16	33.21	1.59	-107.67	1.56	0.7696	0.6413
55906.7672	73.51	2.71	-160.43	2.09	-120.18	1.05	51.88	1.03	0.6811	0.2745
55910.8002	-130.16	2.88	100.96	2.21	-15.96	1.11	-52.73	1.09	0.3294	0.9465
56197.0099	-135.37	2.73	116.48	2.10	32.36	1.06	-104.79	1.03	0.3034	0.6363
56266.8268	69.76	3.80	-149.77	2.92	-122.71	1.47	53.06	1.44	0.8376	0.2696
56608.9494	67.64	3.68	-150.27	2.83	-121.79	1.42	48.33	1.39	0.6632	0.2760
56672.8211	89.04	4.64	-172.64	3.57	-3.77	1.79	-68.09	1.76	0.7676	0.9187
56699.7443	91.74	4.28	-173.27	3.29	-57.27	1.66	-13.60	1.62	0.7711	0.4048
56732.6582	-138.50	4.78	117.79	3.67	7.54	1.85	-78.41	1.81	0.2230	0.8891
56936.0282	-124.81	3.22	101.00	2.47	34.86	1.24	-108.11	1.22	0.3404	0.7757
57001.6916	-130.48	2.41	105.33	1.85	41.24	0.93	-110.90	0.91	0.1770	0.7169
57088.7028	87.13	6.38	-174.30	4.90	-132.59	2.46	60.05	2.41	0.7386	0.2152
57114.6225	-124.49	4.21	101.39	3.24	5.14	1.63	-76.77	1.59	0.3320	0.5341
57121.6335	-136.65	4.67	112.56	3.59	40.67	1.80	-106.58	1.77	0.1974	0.7023
57296.9155	69.25	2.02	-150.51	1.55	0.31	0.78	-70.49	0.76	0.8352	0.9088
57323.8360	67.34	2.32	-153.87	1.79	-62.43	0.90	-5.64	0.88	0.8376	0.3944
57350.7407	68.78	2.10	-153.30	1.61	12.60	0.81	-81.75	0.80	0.8336	0.8774
57390.6960	-125.54	1.97	99.88	1.51	4.14	0.76	-76.14	0.74	0.1634	0.5350
57412.7314	-126.66	2.31	101.63	1.78	-129.52	0.89	61.22	0.87	0.1693	0.2066
57416.7267	80.37	2.63	-164.31	2.02	15.91	1.02	-84.42	1.00	0.8021	0.8724
57432.6346	-134.43	2.44	113.41	1.87	1.51	0.94	-69.86	0.92	0.3037	0.5230
57476.6803	-130.11	3.58	111.41	2.75	18.78	1.38	-87.66	1.35	0.3052	0.8621
57647.9149	-138.57	2.08	117.12	1.60	-63.92	0.81	-5.83	0.79	0.2890	0.3942
57648.9254	84.27	2.25	-168.77	1.73	15.51	0.87	-83.43	0.85	0.7020	0.5625
57653.9942	88.36	2.59	-171.63	1.99	-55.67	1.00	-12.13	0.98	0.7736	0.4071
57679.8731	-118.45	2.27	94.34	1.74	41.04	0.88	-111.09	0.86	0.3503	0.7192
57706.7676	-122.75	2.51	95.61	1.93	-128.21	0.97	61.18	0.95	0.3421	0.2005
57766.5938	87.44	2.36	-163.53	1.82	-120.89	0.91	55.47	0.89	0.7932	0.1690
57794.7257	-135.40	2.10	114.60	1.61	20.54	0.81	-89.59	0.79	0.2907	0.8565

(This table is available in machine-readable form.)

The top panel of Figure 2 shows all timing measurements after subtracting the linear ephemeris from our best-fit global orbital solution described below. They display the obvious LTTE first reported by Wolf et al. (2004) and provide a strong constraint on the elements of the outer orbit. Also shown in the figure is the time history of our other observations. The early CfA spectra were gathered fortuitously near periastron passage.

### 3. Analysis

The configuration of the quadruple V482 Per system is hierarchical, with the outer period being 1000 times longer than

the longest of the inner periods (see below). For the purposes of this work, we will regard this architecture to be sufficiently well represented by three non-interacting Keplerian orbits. The different types of observations available constrain the parameters of the three orbits in different ways and are quite complementary. The approach in this paper is therefore to combine them all into a single solution to make optimal use of the information. There is in fact some redundancy such that some of the elements can be obtained in more than one way, as described below, and this allows one to reduce the number of variables. It is also possible to constrain other properties of the system not usually accessible in non-eclipsing binaries.

**Table 4**  
Heliocentric Radial-velocity Measurements of V482 Per from the Fairborn Observatory

HJD (2,400,000+)	RV <sub>Aa</sub> (km s <sup>-1</sup> )	RV <sub>Ab</sub> (km s <sup>-1</sup> )	RV <sub>Ba</sub> (km s <sup>-1</sup> )	RV <sub>Bb</sub> (km s <sup>-1</sup> )	Phase Aa+Ab	Phase Ba+Bb
55893.8851	-87.6	50.6	-109.8	41.3	0.4161	0.1280
55926.8766	42.2	-108.8	34.3	-102.7	0.8998	0.6252
55947.8192	...	...	-106.5	33.5	...	0.1148
55984.6605	...	...	-126.7	56.4	...	0.2535
56017.6807	...	...	38.4	-108.3	...	0.7555
56188.9963	...	...	-110.9	38.8	...	0.3011
56209.7776	...	...	36.4	-109.1	...	0.7638
56229.7011	67.6	-156.2	...	...	0.6643	...
56265.6515	-111.5	94.7	-86.6	14.0	0.3572	0.0738
56288.9111	63.9	-136.7	...	...	0.8634	...
56328.8122	-124.5	100.5	27.7	-98.0	0.1710	0.5980
56353.6641	-131.4	107.1	39.4	-109.9	0.3280	0.7389
56559.9008	...	...	-100.9	31.2	...	0.1033
56630.6538	...	...	6.8	-77.3	...	0.8925
56649.6758	-142.6	119.1	-78.5	8.6	0.3081	0.0621
56667.6360	73.2	-145.5	-72.4	4.9	0.6484	0.0547
56686.8530	...	...	-126.0	57.7	...	0.2568
56702.7574	...	...	1.9	-70.0	...	0.9068
56931.8161	...	...	-85.9	16.0	...	0.0739
56951.7638	95.0	-171.9	-60.4	-7.6	0.7715	0.3977
56992.0182	-135.6	122.9	-100.8	33.6	0.2235	0.1051
57297.7976	-136.8	123.4	...	...	0.1957	...
57359.7054	...	...	-75.0	5.9	...	0.3712
57401.8024	93.6	-172.9	-69.9	-3.1	0.7026	0.3856
57434.7679	-138.5	105.1	13.7	-80.7	0.1756	0.8785
57464.7014	...	...	16.6	-85.2	...	0.8662
57607.9271	...	...	39.9	-107.6	...	0.7312
57649.8716	-79.1	50.8	37.8	-110.1	0.0887	0.7202
57676.8915	-116.3	77.5	-128.1	62.9	0.1317	0.2224
57694.9427	...	...	-129.2	61.9	...	0.2302
57711.9514	...	...	-77.4	10.5	...	0.0642
57735.8273	-141.5	119.6	...	...	0.2189	...
57789.7710	-148.6	121.2	-58.2	-12.6	0.2657	0.0310
57814.7642	...	...	-130.8	61.0	...	0.1954
57820.7494	...	...	-126.3	58.8	...	0.1927
57833.7036	-140.3	115.2	-87.7	20.1	0.2210	0.3512
57849.6362	87.2	-173.2	...	...	0.7327	...

**Note.** Uncertainties for stars Aa, Ab, Ba, and Bb are 5.4, 3.9, 1.3, and 1.6 km s<sup>-1</sup>, respectively.

(This table is available in machine-readable form.)

### 3.1. Constraints on Orbital Elements

In our initial analysis, our model for the system included only the eclipses of the 2.4 day binary, guided by previous works and the appearance of the light curves. The usual spectroscopic elements for this binary are  $P_A$ ,  $K_{Aa}$ ,  $K_{Ab}$ ,  $e_A$ ,  $\omega_A$ , and  $T_A$ , where the longitude of periastron  $\omega$  refers to the primary (star Aa) and  $T_A$  is a reference time of primary eclipse. The inclination angle is  $i_A$ . There was no obvious evidence in the raw photometry of eclipses of the 6 day binary, despite the fact that preliminary spectroscopic orbital solutions suggested large and nearly equal minimum masses for its components close to what was expected from the temperatures of the stars, indicative of a high inclination angle. Because we measure velocities for all four stars, the outer “binary” (A + B) is effectively double lined, and its velocity semiamplitudes  $K_A$  and  $K_B$  can be determined directly. Under these circumstances, it is possible to infer the inclination angle of the 6 day binary

from elements of the three orbits by

$$\sin^3 i_B = \frac{P_B(1 - e_B^2)^{3/2}(K_{Ba} + K_{Bb})^3 K_B}{P_A(1 - e_A^2)^{3/2}(K_{Aa} + K_{Ab})^3 K_A} \sin^3 i_A, \quad (1)$$

and thus to obtain the absolute masses of the four stars.

It is also possible to infer the inclination angle of the outer orbit, which is given in terms of other known elements, by

$$\sin^3 i_{AB} = \frac{P_{AB}(1 - e_{AB}^2)^{3/2}(K_A + K_B)^2 K_B}{P_A(1 - e_A^2)^{3/2}(K_{Aa} + K_{Ab})^3} \sin^3 i_A, \quad (2)$$

where the subscripts “AB” refer to the outer orbit.

Closer examination subsequently revealed very shallow eclipses of the 6 day binary precisely at the phases expected from the spectroscopic orbit (see below), allowing a direct measurement of  $i_B$  and enabling the absolute masses of its components to be determined another way (without recourse to the outer orbit). This redundancy yields a relation between the

**Table 5**  
Times of Minimum Light for V482 Per

HJD (2,400,000+)	$\sigma$ (days)	Type	( $O - C$ ) (days)	Year	Source
47565.3737	...	2	-0.00286	1989.104	1
47823.5048	...	1	-0.00420	1989.811	1
47840.636	...	1	-0.00026	1989.858	1
47850.4210	...	1	-0.00225	1989.885	1
47943.4012	...	1	+0.00150	1990.139	1

**Note.** Measurement errors ( $\sigma$ ) are listed as published, when available. Uncertainties for the timings with no published errors are assumed to be 0.0027 days for primary minima and 0.0010 days for secondary minima (see Section 3.2). “Type” is 1 for a primary eclipse, 2 for a secondary eclipse.  $O - C$  residuals are computed from the combined fit described in Section 3. Sources for the times of minimum light are (1) Agerer & Lichtenknecker (1991); (2) Hübscher et al. (1991); (3) Hübscher et al. (1992); (4) Hübscher et al. (1993); (5) Hübscher et al. (1994); (6) Agerer & Hübscher (1995); (7) Agerer & Hübscher (1996); (8) Agerer & Hübscher (1997); (9) Agerer & Hübscher (1998); (10) Agerer et al. (1999); (11) Paschke (2017); (12) Lacy (2002); (13) Lacy (2003); (14) Agerer & Hübscher (2003); (15) Kotková & Wolf (2006); (16) Zejda (2004); (17) Lacy (2004); (18) Lacy (2006); (19) Brát et al. (2007); (20) Lacy (2007); (21) Hübscher & Walter (2007); (22) Lacy (2009); (23) Yilmaz et al. (2009); (24) Hübscher et al. (2009a); (25) Hübscher et al. (2009b); (26) Diethelm (2009); (27) Lacy (2011); (28) Diethelm (2011a); (29) Diethelm (2011b); (30) Hübscher et al. (2012); (31) Liakos & Niarchos (2011); (32) Lacy (2012); (33) Lacy (2013); (34) Diethelm (2013); (35) Hübscher & Lehmann (2015); (36) Juryšek et al. (2017); (37) Zasche et al. (2017).

(This table is available in its entirety in machine-readable form.)

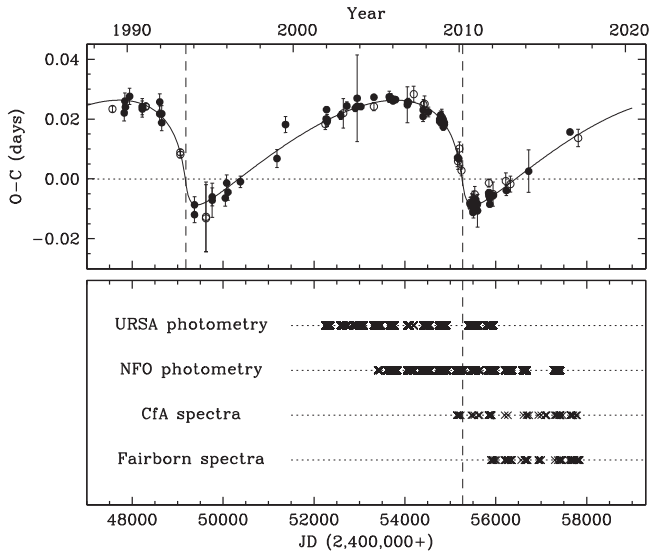


**Figure 2.** Top: times of minimum light from Table 5 with our best-fit linear ephemeris subtracted out, to yield observed minus computed ( $O - C$ ) residuals showing the light-travel time effect. Filled and open symbols represent primary and secondary minima, respectively, and the solid curve is our best-fit model for the light-travel effect described in Section 3.2. The vertical dashed lines indicate times of periastron passage in the outer orbit. Bottom: time history of our photometric and spectroscopic observations for comparison with the eclipse timings.

semiamplitudes of the outer orbit (from Equation (1)):

$$K_B = \frac{P_A(1 - e_A^2)^{3/2}(K_{Aa} + K_{Ab})^3 \sin^3 i_B}{P_B(1 - e_B^2)^{3/2}(K_{Ba} + K_{Bb})^3 \sin^3 i_A} K_A, \quad (3)$$

and it can be used to eliminate either  $K_A$  or  $K_B$  as adjustable variables. Our spectroscopic observations alone give us relatively weak constraints on these semiamplitudes because the radial velocities cover only a fraction of the outer orbit (although they do partially sample periastron passage). On the other hand, the times of minimum light of Section 2.3 span more than one cycle of the outer orbit and help to pin down  $K_A$ , with the net effect that this quantity is better constrained by the observations than  $K_B$ . Consequently, we have chosen to use Equation (3) to eliminate  $K_B$ , retaining only  $K_A$  as a free parameter.

### 3.2. Solution

Both inner binaries are well detached. We modeled their light curves using the Nelson–Davis–Ezetz formalism (Popper & Etzel 1981; Etzel 1981), as implemented in the widely used EBOP code, which is adequate for systems such as these with nearly spherical stars. In order to allow the flexibility to incorporate the various constraints described below, and to combine all observations together and solve for all parameters simultaneously, we made use of a version of EBOP from Irwin et al. (2011) that is especially useful within the framework of the Markov Chain Monte Carlo (MCMC) methodology we apply here.<sup>6</sup> The relative weighting of the different data sets relied on the uncertainties established for each type of observation, as described earlier, and we verified that modest changes in those uncertainties did not affect the results significantly.

In addition to the ephemeris ( $P_A$  and the time of primary minimum  $T_A$ ), the light-curve elements for the 2.4 day binary are the  $V$ -band central surface brightness ratio between the secondary and the primary  $J_A$ , the sum of the relative radii  $r_{Aa} + r_{Ab}$ , the radius ratio  $k_A \equiv r_{Ab}/r_{Aa}$ , the cosine of the inclination angle  $\cos i_A$ , the eccentricity parameters  $\sqrt{e_A} \cos \omega_A$  and  $\sqrt{e_A} \sin \omega_A$ , and a third-light parameter  $L_3$  to account for the dilution effect produced by the flux from the other binary, where  $L_3$  is the fractional light contribution relative to the total. Similar adjustable light-curve parameters were considered for the 6 day binary, once we discovered that it is also eclipsing. Both sets of parameters were solved for simultaneously, with the third-light parameter for binary B being simply  $1 - L_3$ . We also solved for separate out-of-eclipse magnitude levels for URSA and NFO,  $m_{\text{URSA}}$  and  $m_{\text{NFO}}$ , and allowed for separate scale factors applied to the estimated internal photometric errors from these two telescopes,  $f_{\text{URSA}}$  and  $f_{\text{NFO}}$ , which were set initially to values of 0.008 mag and 0.012 mag, respectively, from preliminary fits. Test solutions indicated negligible eccentricity in the 2.4 day orbit, so for the final fit we considered it to be circular.

Limb darkening was represented with a linear law, as experiments with a two-parameter quadratic law gave no improvement. The  $V$ -band coefficients for the four components were taken from the tables of Claret & Bloemen (2011) in accordance with the stellar properties reported earlier. They are 0.451, 0.494, 0.597, and 0.597 for stars Aa, Ab, Ba, and Bb, respectively. Gravity-darkening coefficients were calculated as described in Torres et al. (2017), and were set to 0.672, 0.727, 0.886, and 0.886.

<sup>6</sup> <https://github.com/mdwarfgeek/eb>

Additional spectroscopic parameters of the fit are the center-of-mass velocity of the quadruple system  $\gamma$ ; the velocity semiamplitudes of the inner orbits  $K_{Aa}$ ,  $K_{Ab}$ ,  $K_{Ba}$ , and  $K_{Bb}$ ; the period and reference epoch of periastron passage of the outer orbit  $P_{AB}$  and  $T_{AB}$ ; the eccentricity parameters  $\sqrt{e_{AB}} \cos \omega_{AB}$  and  $\sqrt{e_{AB}} \sin \omega_{AB}$  (where  $\omega_{AB}$  corresponds to the ‘‘primary’’ in the outer orbit, i.e., the A binary); and the velocity semiamplitude  $K_A$  mentioned earlier, tracing the motion of the center of mass of the A binary. Additionally, we allowed for a possible difference  $\Delta RV$  in the velocity zero points of our CfA and Fairborn observations. Initially, we also considered possible offsets between the primary and secondary velocity zero points within each inner binary, which may result, e.g., from template mismatch in the CfA determinations. We found these offsets to be insignificant in early tests, and therefore dropped them for the final solutions.

The periodic variations in the times of minimum light of the A binary were modeled as mentioned earlier with the third-body formalism of Irwin (1952, 1959). For all practical purposes, these measurements may be assumed to correspond to times of conjunction, as the difference is negligible in our case. The LTTE in the outer orbit was fully accounted for in the treatment of the radial-velocity motion in the inner orbits and for the light-curve solutions. This was done by adjusting the individual times of observation at each step of the iterations based on the current values of the outer elements. All reference epochs from our solution ( $T_A$ ,  $T_B$ ,  $T_{AB}$ ) are in the frame of the center of mass of the quadruple system and were defined to be near the average epoch of all observations, to minimize correlations.

Our method of solution for V482 Per used the `emcee`<sup>7</sup> code of Foreman-Mackey et al. (2013), which is a Python implementation of the affine-invariant MCMC ensemble sampler proposed by Goodman & Weare (2010). We used 300 walkers and uniform priors over suitable ranges for most elements. Initial solutions showed that the radius ratio  $k_B$  in the 6 day binary was poorly constrained from photometry alone, and converged to unrealistically low values under 0.5 for two stars that are in fact very similar in mass and temperature. A similar problem occurred with the central surface brightness ratio  $J_B$ . This is not surprising given the very shallow eclipses caused by heavy dilution from the much brighter 2.4 day binary, the presence of instrumental errors in one of our photometric data sets (NFO) that may be distorting the eclipse shapes and depths (see below), and the partial nature of the eclipses of two similar stars (see, e.g., Andersen et al. 1991).

To overcome this difficulty, we made use of the measured spectroscopic light ratio between stars Ba and Bb ( $\ell_{Bb}/\ell_{Ba} = 0.99 \pm 0.05$ , the weighted average of our two determinations from Section 2.2), which is strongly correlated with the radius ratio ( $\ell_{Bb}/\ell_{Ba} \propto k_B^2$ ), and applied it as a Gaussian prior on the light ratio to constrain the fit. Because the two stars appear to have essentially identical temperatures, we also used a Gaussian prior of  $1.00 \pm 0.02$  on the central surface brightness ratio  $J_B$ . An additional constraint imposed on our solutions was that  $\sin^3 i_{AB}$ , as given by Equation (2), be strictly less than unity (with  $K_B$  computed from Equation (3)). Convergence was checked by examining the chains visually and verifying that the Gelman-Rubin statistic (Gelman &

**Table 6**  
Combined Orbital Solution for V482 Per

Parameter	Value and Uncertainty
$P_A$ (days)	$2.44675265 \pm 0.00000027$
$T_A$ (HJD) <sup>a</sup>	$2,454,848.10959 \pm 0.00032$
$J_A$	$0.778 \pm 0.047$
$r_{Aa} + r_{Ab}$	$0.3560 \pm 0.0053$
$k_A \equiv r_{Ab}/r_{Aa}$	$0.644 \pm 0.021$
$\cos i_A$	$0.119 \pm 0.018$
$L_3^b$	$0.145 \pm 0.049$
$f_{URSA}$	$0.9929 \pm 0.0069$
$f_{NFO}$	$1.0596 \pm 0.0073$
$m_{URSA}$ (mag)	$0.0312 \pm 0.0012$
$m_{NFO}$ (mag)	$0.3269 \pm 0.0010$
$P_B$ (days)	$6.001749 \pm 0.000023$
$T_B$ (HJD) <sup>a</sup>	$2,454,848.8326 \pm 0.0071$
$J_B$	$0.973 \pm 0.043$
$r_{Ba} + r_{Bb}$	$0.136 \pm 0.012$
$k_B \equiv r_{Bb}/r_{Ba}$	$1.009 \pm 0.044$
$\sqrt{e_B} \cos \omega_B$	$-0.3317 \pm 0.0046$
$\sqrt{e_B} \sin \omega_B$	$-0.0164 \pm 0.0095$
$\dot{\omega}_B$ ( $10^{-5}$ rad day <sup>-1</sup> )	$-2.89 \pm 0.62$
$\cos i_B$	$0.081 \pm 0.018$
$\gamma$ (km s <sup>-1</sup> )	$-30.03 \pm 0.14$
$\Delta RV$ (km s <sup>-1</sup> ) <sup>c</sup>	$-0.21 \pm 0.22$
$K_{Aa}$ (km s <sup>-1</sup> )	$115.60 \pm 0.86$
$K_{Ab}$ (km s <sup>-1</sup> )	$147.22 \pm 0.52$
$K_{Ba}$ (km s <sup>-1</sup> )	$85.02 \pm 0.34$
$K_{Bb}$ (km s <sup>-1</sup> )	$85.72 \pm 0.35$
$P_{AB}$ (days)	$6089 \pm 29$
$T_{AB}$ (HJD) <sup>a</sup>	$2,455,271.5 \pm 5.2$
$K_A$ (km s <sup>-1</sup> )	$17.20 \pm 0.75$
$\sqrt{e_{AB}} \cos \omega_{AB}$	$-0.8631 \pm 0.0066$
$\sqrt{e_{AB}} \sin \omega_{AB}$	$-0.3291 \pm 0.0097$

**Notes.** The values reported correspond to the mode from the MCMC posterior distributions. The uncertainties come from the residual permutation procedure described in the text.

<sup>a</sup>  $T_A$  and  $T_B$  are the reference times of primary eclipse in the 2.4 day and 6 day binaries (eclipse of stars Aa and Ba), and  $T_{AB}$  is the reference time of periastron passage in the outer orbit.

<sup>b</sup> Fraction of the light contributed by stars Ba+Bb.

<sup>c</sup> Zero-point difference between the CfA and Fairborn velocity frames, in the sense of Fairborn minus CfA.

Rubin 1992; Brooks & Gelman 1997) was smaller than 1.05 for all adjustable parameters.

Early solutions resulted in a satisfactory fit to most of the observations except for the velocities of the 6 day binary, which showed an obvious pattern of phase-dependent residuals far in excess of the estimated uncertainties. It was eventually found that this could be eliminated by allowing for apsidal motion in this slightly eccentric orbit. The addition of  $\dot{\omega}_B$  as a free parameter to our fit did indeed yield a highly significant value of about 60 deg per century, but with a sign that indicated precession in the direction *opposite* to the orbital motion. We discuss this further below. With allowance for apsidal motion, the orbital period of the B binary we solved for is strictly the sidereal period, which in this case is longer than the anomalistic period for the reason indicated. The fitted value of  $\omega_B$  is for the reference epoch of primary eclipse,  $T_B$ .

The resulting 31 parameters from our MCMC solution are presented in Table 6, and other properties derived from the

<sup>7</sup> <http://dan.iel.fm/emcee>



**Table 7**  
Derived Properties for V482 Per

Parameter	Value and Uncertainty
$r_{Aa}$	$0.2166 \pm 0.0021$
$r_{Ab}$	$0.1393 \pm 0.0048$
$r_{Ba}$	$0.0681 \pm 0.0058$
$r_{Bb}$	$0.0686 \pm 0.0061$
$K_{LTTE,A}$ (minutes) <sup>a</sup>	$25.24 \pm 0.25$
$P_{B,anom}$ (days) <sup>b</sup>	$6.001583 \pm 0.000015$
$T_{peri,B}$ (HJD) <sup>c</sup>	$2,454,850.171 \pm 0.029$
$\dot{\omega}_B$ (deg century <sup>-1</sup> )	$-60 \pm 13$
$U_B$ (years) <sup>d</sup>	$590 \pm 210$
$e_B$	$0.1103 \pm 0.0031$
$\omega_B$ (degrees) <sup>e</sup>	$182.9 \pm 1.6$
$\phi_B$ <sup>f</sup>	$0.4300 \pm 0.0020$
$P_{AB}$ (years)	$16.672 \pm 0.079$
$K_B$ (km s <sup>-1</sup> ) <sup>g</sup>	$26.4 \pm 1.2$
$e_{AB}$	$0.8533 \pm 0.0084$
$\omega_{AB}$ (degrees) <sup>e</sup>	$200.90 \pm 0.67$
$\sin^3 i_{AB}$ <sup>h</sup>	$0.958 \pm 0.056$
$i_{AB}$ (degrees)	$79.6 \pm 6.4$
$i_A$ (degrees)	$83.2 \pm 1.0$
$i_B$ (degrees)	$85.3 \pm 1.1$
$\ell_{Ab}/\ell_{Aa}$	$0.324 \pm 0.029$
$\ell_{Ba}/\ell_{Aa}$	$0.112 \pm 0.042$
$\ell_{Bb}/\ell_{Aa}$	$0.113 \pm 0.042$
$\ell_{Bb}/\ell_{Ba}$	$1.000 \pm 0.019$
$\ell_B/\ell_A$	$0.169 \pm 0.065$
$q_A \equiv M_{Ab}/M_{Aa}$	$0.7853 \pm 0.0065$
$q_B \equiv M_{Bb}/M_{Ba}$	$0.9918 \pm 0.0050$
$q_{AB} \equiv M_B/M_A$	$0.652 \pm 0.010$
$a_A$ ( $R_\odot$ )	$12.800 \pm 0.050$
$a_B$ ( $R_\odot$ )	$20.199 \pm 0.067$
$a_{AB}$ (au)	$12.926 \pm 0.054$

**Notes.** The values reported correspond to the mode from the MCMC posterior distributions. The uncertainties come from the residual permutation procedure described in the text. The physical constants used to calculate the semimajor axes conform to IAU recommendations from 2015 Resolution B3 (see Prša et al. 2016).

<sup>a</sup> Semiamplitude of the light-travel time effect on the eclipse timings of the 2.4 day binary, caused by motion in the orbit around the center of mass with the 6 day binary.

<sup>b</sup> Anomalous period in the 6 day binary.

<sup>c</sup> Time of periastron passage for the 6 day binary.

<sup>d</sup> Apsidal period in the 6 day binary.

<sup>e</sup> Following the spectroscopic convention, the angle  $\omega_B$  corresponds to star Ba, and  $\omega_{AB}$  to binary A in the wide orbit.

<sup>f</sup> Phase of the secondary eclipse in the 6 day binary orbit.

<sup>g</sup> Computed with Equation (3).

<sup>h</sup> Computed with Equation (2).

fitted parameters are listed in Table 7.<sup>8</sup> The formal uncertainties returned by the procedure were found to be too small because it does not account for time-correlated noise in our observations (“red” noise), which is significant particularly in the differential NFO photometry, as discussed below. To address this concern, we carried out a residual permutation (“prayer bead”) exercise

<sup>8</sup> For quantities that are combinations of others, our choice to report the mode of all posterior distributions can result in small, unavoidable differences between the mode of the derived quantity and the results one would compute directly from the modal values of the independent variables (such as  $r_{Aa}$  or  $r_{Ab}$  from the radius sum and  $k_A$ ).

in which we shifted the residuals from our original fit by an arbitrary number of time indices (for all data sets), added them back into the model curves at each time of observation (with wraparound over each data set), and then performed the MCMC adjustment again on the synthetic data sets. This preserves the pattern of the correlated noise. We also perturbed both the limb-darkening and gravity-darkening coefficients by adding Gaussian noise with  $\sigma = 0.1$ . We repeated this operation 100 times and adopted the scatter from the distribution of results for each adjusted and derived parameter as the final uncertainty. We consider these error estimates to be more realistic: they are typically 2–10 times larger than the internal errors.

As may be expected from the complexity of the solution, several of the fitted parameters are quite strongly correlated (for example,  $\{r_{Aa} + r_{Ab}, k_A\}$ ,  $\{J_A, \cos i_A, L_3\}$ ,  $\{r_{Ba} + r_{Bb}, \cos i_B\}$ ,  $\{P_B, \dot{\omega}_B\}$ ,  $\{J_A, \cos i_A, \cos i_B, L_3\}$ , etc.). We used the chains from our Monte Carlo analysis to illustrate this in Figure 3, for some of the variables with the strongest correlations. Others not shown that are also correlated include  $\{P_{AB}, K_A, \sqrt{e_{AB}} \cos \omega_{AB}, \sqrt{e_{AB}} \sin \omega_{AB}\}$  and  $\{\gamma, \Delta RV\}$ .

Despite the use of the MCMC method, which is designed to explore the high-dimensional parameter space more thoroughly than traditional least-squares techniques, the uniqueness of a solution with as many adjustable parameters as we have is generally difficult to prove, particularly in the presence of significant correlations among some of the variables, as shown above. We investigated this by repeating our solution using different sets of initial values for the parameters, which causes MCMC to sweep the parameter space in a different way each time. We found that in all cases the results were consistent with those we report.

Figure 4 shows our differential photometry compared with the best-fit model for the 2.4 day binary. The eclipses in the 6 day binary have been removed from the data. Conversely, subtracting the variations in the 2.4 day binary from the original data gives the residuals seen in Figure 5, displayed separately for the URSA and NFO telescopes. An enlargement of the eclipse regions is shown in Figure 6 (top and middle panels) along with the best-fit eclipse model for the 6 day binary. Despite having only partial coverage near phase 0.0, the URSA observations show clear evidence of dips in the light curve at the precise locations where eclipses could occur in this binary, according to the spectroscopic orbit (vertical dotted lines). On the other hand, the evidence for eclipses in the NFO data is marginal. As discussed by Lacy et al. (2008), NFO observations are known to suffer from small but significant offsets from night to night that appear to be up to a few hundredths of a magnitude for V482 Per. They are due to a combination of centering errors and responsivity variations across the field of view. The URSA observations are much less affected. The NFO systematics are clearly visible in Figures 5 and 6, and are in fact comparable to the size of the eclipses in the 6 day binary, which are measured to be only 0.023 mag deep. As a result, the evidence for eclipses in binary B is not particularly compelling from the NFO data alone, especially with their lack of coverage near the secondary minimum. These features might have been missed entirely were it not for the independent URSA data and the critical information from spectroscopy. The bottom panels of Figure 6 show the URSA and NFO observations combined, which provide full coverage of both eclipses. The primary and secondary minima are equally deep.

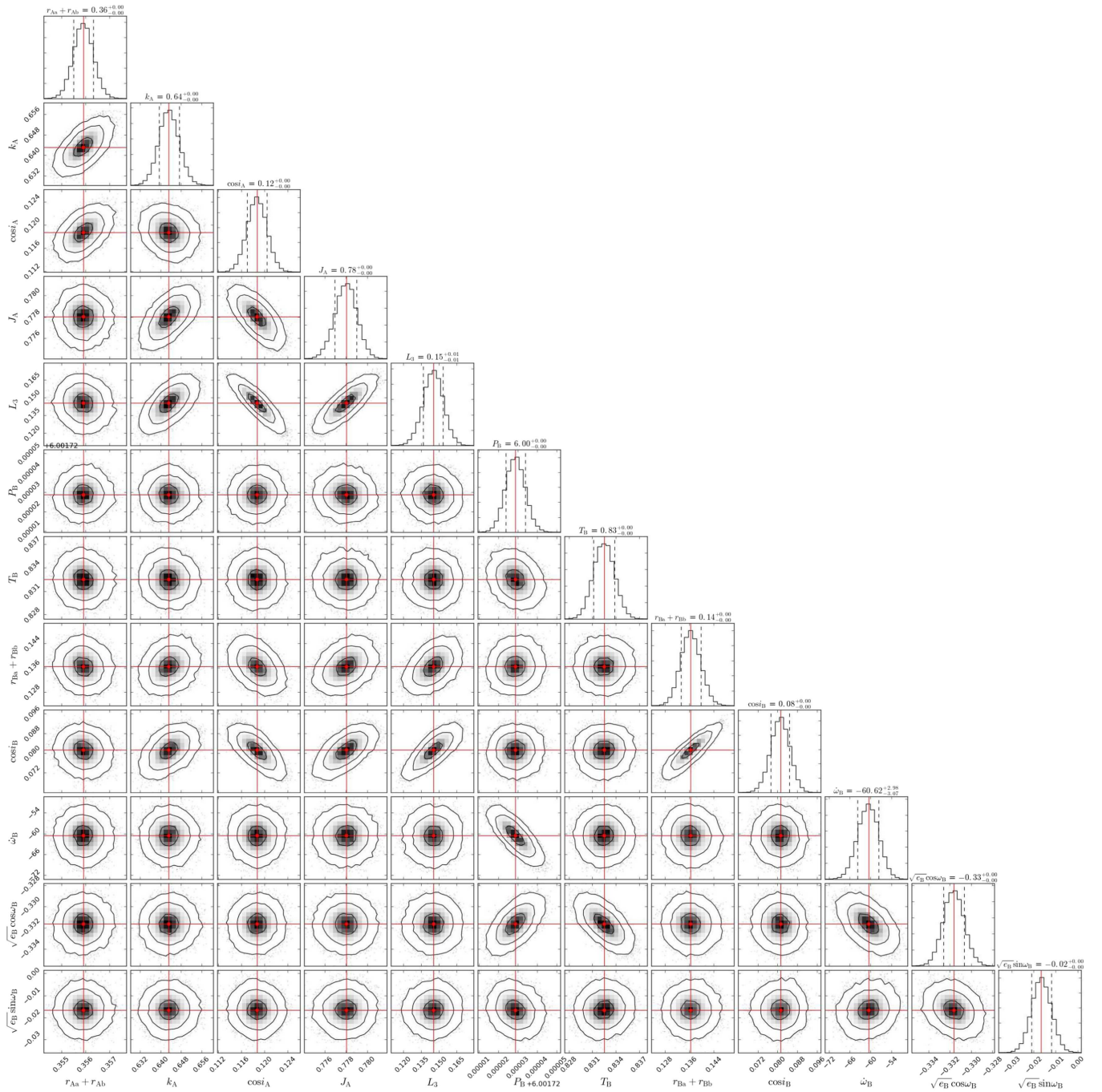


**Figure 3.** “Corner plot” (Foreman-Mackey 2016; <https://github.com/dfm/corner.py>) for V482 Per illustrating the correlations among a selection of the fitted parameters of our solution. Contour levels correspond to  $1\sigma$ ,  $2\sigma$ , and  $3\sigma$ , and the histograms on the diagonal represent the posterior distribution for each parameter, with the mode and internal 68% confidence levels indicated. More realistic errors are discussed in the text.

Our detection of statistically significant apsidal precession in the 6 day binary in the direction opposite to that of the orbital motion should be taken with caution. In principle, such an effect may well arise from the hierarchical configuration of the V482 Per system, with a highly eccentric outer orbit that could lead to dynamical interactions between the inner binaries (see Section 6). However, the presence of systematic errors in at least one of our photometric data sets that are of the same order as the depths of the shallow eclipses of the 6 day binary, combined with the small number of nights in which the eclipses were observed, have the potential to bias the measurement of  $\omega_B$ , although it is unclear by how much. Unfortunately, the data

in hand are less than optimal for an independent check as both the URSA and NFO observations each miss one of the eclipses. A solution without the NFO data still indicated a significant negative apsidal motion. Additional independent observations are highly desirable to confirm this result. In any case, we note that the absolute dimensions of the stars (masses, radii) reported below are unaffected by  $\omega_B$ .

The spectroscopic observations of the 2.4 and 6 day binary components are shown in Figures 7 and 8, along with the best-fit models and residuals. In each case, we subtracted the motion in the 16 year outer orbit for display purposes. The spectroscopic coverage of the outer orbit is illustrated in Figure 9. The

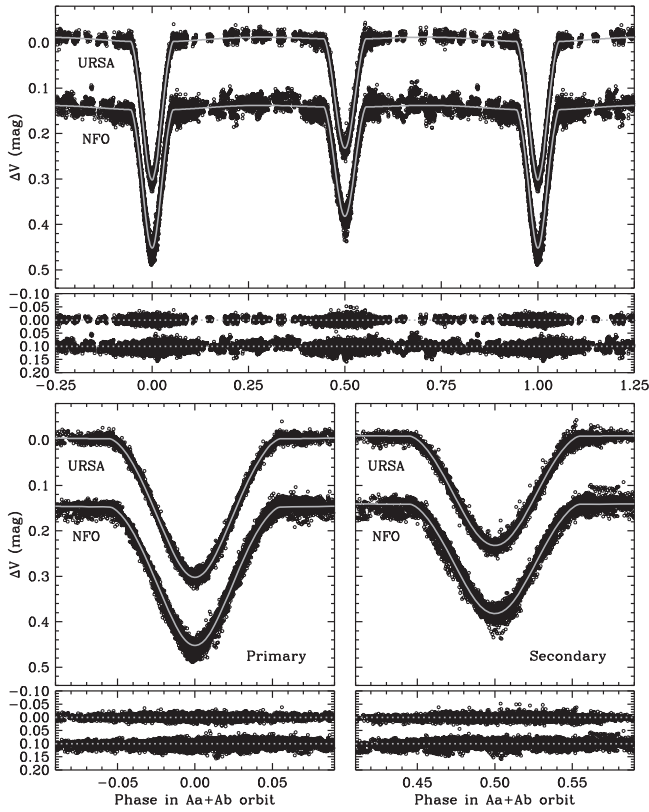


**Figure 4.** Differential V-band photometry of V482 Per from the URSA and NFO telescopes, along with our best-fit eclipse model for the 2.4 day binary. Enlargements of the primary and secondary minima are also shown. Residuals are displayed beneath each panel. The NFO data and residuals are offset vertically for clarity, and the eclipses of the 6 day binary have been removed from the observations.

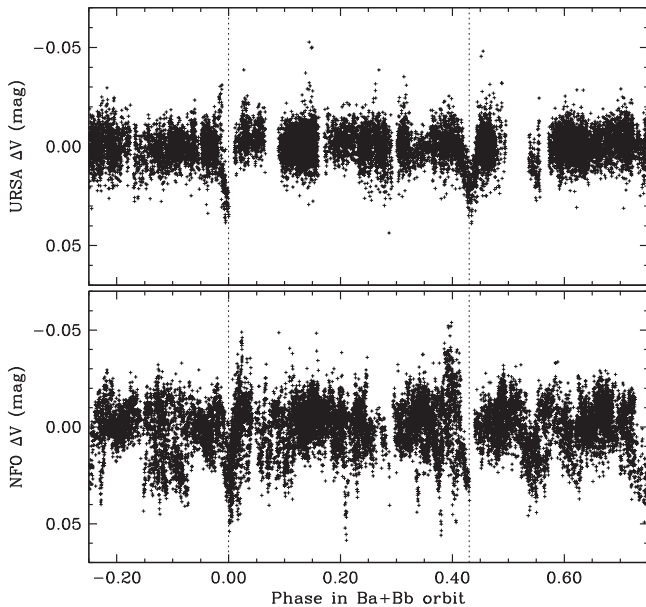


**Figure 5.** Residuals from the URSA and NFO observations after subtracting the variations in the 2.4 day binary based on our global best-fit model.

symbols represent instantaneous measurements of the radial velocity of the center of mass of each binary, calculated by taking the weighted average of the individual primary and secondary velocity residuals after removing the motion in the inner orbits. The early CfA observations are seen to have been

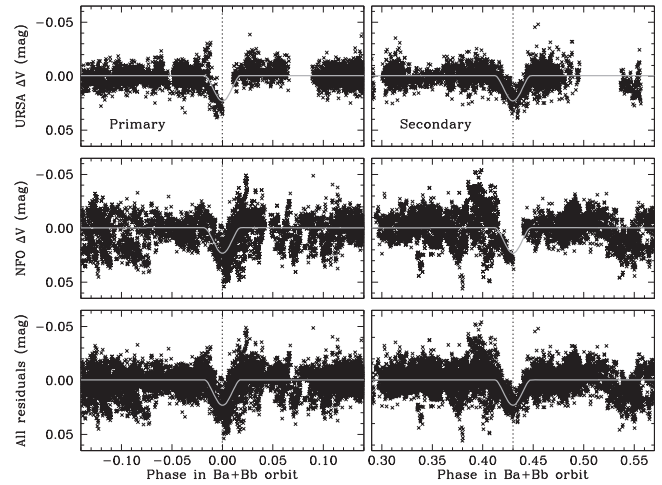


**Figure 6.** Enlargement of Figure 5 around the eclipse regions, along with our best-fit model for the 6 day binary. The observations are combined in the lower panels.

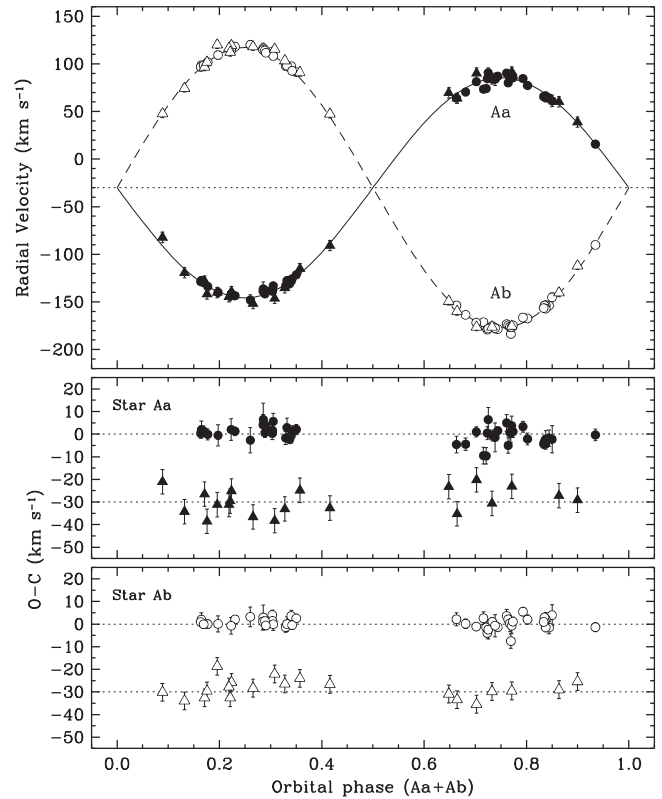


**Figure 7.** Radial-velocity observations of V482 Per in the 2.4 day binary with our best-fit model. Motion in the outer orbit has been subtracted. The dotted line represents the center-of-mass velocity of the quadruple system. Residuals are shown at the bottom separately for the CfA and Fairborn measurements (circles and triangles, respectively).

taken near the important periastron phase. Finally, the fit to the times of minimum light for the 2.4 day binary may be seen in Figure 2, presented earlier.

#### 4. Physical Properties

In Table 8, we summarize the physical properties of the four stars in V482 Per derived from the parameters of our orbital solution in the previous section. Stars Ba and Bb have nearly



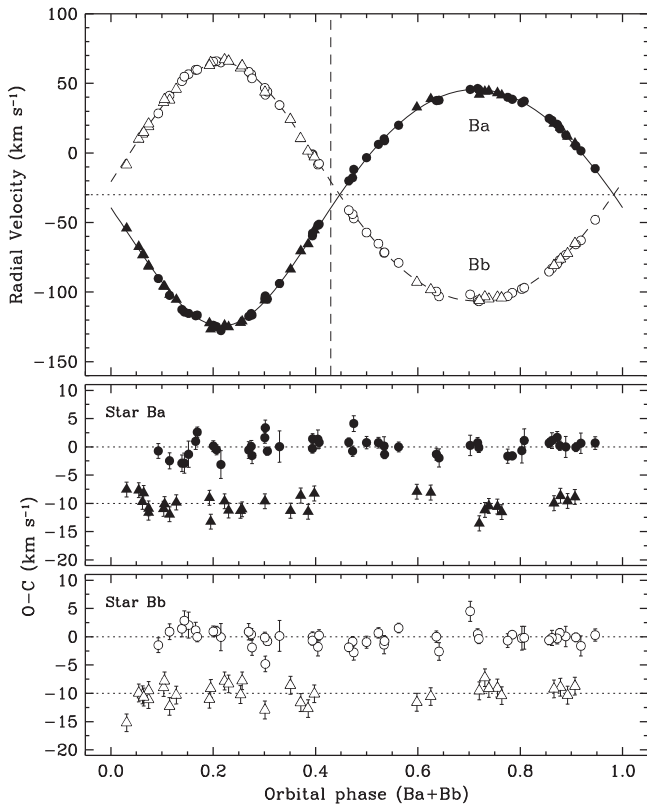


**Figure 8.** Same as Figure 7 for the 6 day binary. The vertical dashed line indicates the phase of the secondary eclipse at  $\phi_B = 0.4300 \pm 0.0020$ , according to our fit.

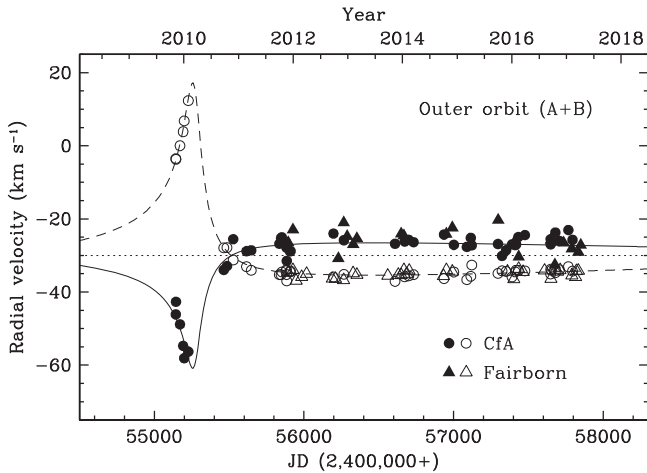


**Figure 9.** Radial-velocity motion of the centers of mass of the 2.4 and 6 day binaries in the outer 16 year orbit. The individual measurements for each star have been corrected for the motion in the corresponding inner binary, and then weight-averaged together for display purposes and represented by a single symbol. Filled symbols correspond to Aa+Ab, and open ones to Ba+Bb. The solid curves represent our best fit, and the dashed line marks the center-of-mass velocity of the quadruple system.

identical masses, and their radii are indistinguishable within the errors.

The distance to each binary was computed independently relying on bolometric corrections from Flower (1996), the out-of-eclipse magnitude of the system ( $V = 10.250 \pm 0.032$ ; Zacharias et al. 2015), our third-light estimate from Table 6, and (distance-dependent) reddening estimates from Green et al. (2015) determined by iterations to reach convergence. The

**Table 8**  
Physical Properties of the V482 Per Components

Parameter	Primary	Secondary
Binary Aa+Ab		
$M (M_\odot)$	$2.634 \pm 0.029$	$2.068 \pm 0.030$
$R (R_\odot)$	$2.774 \pm 0.031$	$1.784 \pm 0.062$
$\log g$ (cgs)	$3.9727 \pm 0.0083$	$4.251 \pm 0.030$
$T_{\text{eff}}$ (K)	$10600 \pm 200$	$9600 \pm 200$
$L/L_\odot$	$87.5 \pm 6.9$	$24.4 \pm 2.6$
$BC_V$ (mag) <sup>a</sup>	$-0.38 \pm 0.11$	$-0.17 \pm 0.11$
$M_{\text{bol}}$ (mag) <sup>b</sup>	$-0.123 \pm 0.085$	$1.27 \pm 0.12$
$M_V$ (mag)	$0.26 \pm 0.11$	$1.43 \pm 0.13$
$E(B - V)$ (mag)		$0.36 \pm 0.06$
$m - M$ (mag)		$9.36 \pm 0.22$
Distance (pc) <sup>c</sup>		$746 \pm 75$
Parallax (mas)		$1.34 \pm 0.14$
$v_{\text{sync}} \sin i$ (km s <sup>-1</sup> ) <sup>d</sup>	$56.96 \pm 0.65$	$36.63 \pm 0.65$
$v \sin i$ (km s <sup>-1</sup> ) <sup>e</sup>	$60 \pm 5$	$40 \pm 5$
$v \sin i$ (km s <sup>-1</sup> ) <sup>e</sup>	$59 \pm 5$	$39 \pm 3$
Binary Ba+Bb		
$M (M_\odot)$	$1.540 \pm 0.016$	$1.528 \pm 0.016$
$R (R_\odot)$	$1.37 \pm 0.12$	$1.39 \pm 0.13$
$\log g$ (cgs)	$4.350 \pm 0.073$	$4.338 \pm 0.077$
$T_{\text{eff}}$ (K)	$7600 \pm 300$	$7600 \pm 300$
$L/L_\odot$	$5.6 \pm 1.3$	$5.8 \pm 1.4$
$BC_V$ (mag) <sup>a</sup>	$+0.03 \pm 0.10$	$+0.03 \pm 0.10$
$M_{\text{bol}}$ (mag) <sup>b</sup>	$2.85 \pm 0.25$	$2.82 \pm 0.26$
$M_V$ (mag)	$2.82 \pm 0.27$	$2.79 \pm 0.28$
$E(B - V)$ (mag)		$0.34 \pm 0.08$
$m - M$ (mag)		$9.24 \pm 0.50$
Distance (pc) <sup>c</sup>		$700 \pm 170$
Parallax (mas)		$1.42 \pm 0.32$
$v_{\text{sync}} \sin i$ (km s <sup>-1</sup> ) <sup>d</sup>	$11.5 \pm 1.0$	$11.7 \pm 1.0$
$v_{\text{psync}} \sin i$ (km s <sup>-1</sup> ) <sup>d</sup>	$12.4 \pm 1.1$	$12.5 \pm 1.2$
$v \sin i$ (km s <sup>-1</sup> ) <sup>e</sup>	$12 \pm 2$	$12 \pm 2$
$v \sin i$ (km s <sup>-1</sup> ) <sup>e</sup>	$11 \pm 2$	$13 \pm 2$

**Notes.**

<sup>a</sup> Bolometric corrections from Flower (1996), with a contribution of 0.10 mag added in quadrature to the uncertainty from the temperatures.

<sup>b</sup> Uses  $M_{\text{bol}}^\odot = 4.732$  for consistency with the adopted table of bolometric corrections (see Torres 2010).

<sup>c</sup> Relies on the luminosities, the apparent magnitude of V482 Per out of eclipse ( $V = 10.250 \pm 0.032$ ; Zacharias et al. 2015), and bolometric corrections.

<sup>d</sup> Projected synchronous and pseudo-synchronous rotational velocities.

<sup>e</sup> Measured values from our CfA and Fairborn spectra.

reddening values for the two binaries are in good agreement, as are the derived distances. Similar results for the distance were obtained using the radiative flux scale and absolute  $V$  magnitude calibration of Popper (1980). We note that the adopted reddening values from Green et al. (2015) are different (larger) from most estimates from other sources (Hakkila et al. 1997; Schlegel et al. 1998; Drimmel et al. 2003; Amôres & Lépine 2005), which is possibly explained by uncertainties due to the low Galactic latitude of the object ( $-2^\circ.4$ ). The parallax estimates for the two binaries are formally two to four times more precise than the entry for V482 Per in the *Gaia*/DR1 catalog (Lindegren et al. 2016),  $\pi_{\text{DR1}} = 0.56 \pm 0.57$  mas.

The measured  $v \sin i$  values for the stars in the 2.4 day binary are consistent with estimates for synchronous rotation ( $v_{\text{sync}} \sin i$ ), while those for the 6 day binary cannot distinguish



between synchronous and pseudo-synchronous rotation (Hut 1981).

The masses of all four components are formally determined to better than 1.5%, and the radii of stars Aa and Ab to 1.1% and 3.5%, respectively. The radii of stars Ba and Bb are considerably worse ( $\sim 9\%$ ), largely on account of systematic errors in the observations (“red noise”). Because of the complicated nature of the orbital solution, we consider the radii to be less robust than the masses, and systematic errors that are difficult to quantify may contribute further to the uncertainties we have reported. Although some external information was already used above to impose priors on our fit and strengthen the determination of otherwise poorly constrained quantities related to the 6 day binary ( $k_B$ ,  $J_B$ ), the independent constraints we have available to check the accuracy of some of the derived properties for the 2.4 day binary are relatively weak. For example, if we make the reasonable assumption that the spin axes of the stars in the 2.4 day binary are parallel to the orbital axis and that their rotations are synchronized with the orbital motion, as seems to be the case (see above), then the ratio of our measured  $v \sin i$  values for the components should be equal to the radius ratio  $k_A$ . The projected rotational velocities from our Fairborn spectra yield  $v_{Ab} \sin i / v_{Aa} \sin i = 0.66 \pm 0.08$ , which agrees with the much more precise  $k_A$  value listed in Table 6. The estimate from the CfA spectra ( $0.67 \pm 0.10$ ) is even more uncertain and therefore less useful, but still agrees.

Our spectroscopic light ratios from the CfA spectra allow further checks. The  $\ell_{Ba}/\ell_{Aa}$  and  $\ell_{Bb}/\ell_{Aa}$  values, converted from the mean wavelength of  $5188 \text{ \AA}$  to the  $V$  band<sup>9</sup> yield a ratio of about 0.10, which is not far from the determinations listed in Table 7 ( $\sim 0.11$ ). However, we find a discrepancy in the Ab/Aa ratio. Our spectroscopic estimate from Section 2.2 converted to the  $V$  band is  $0.55 \pm 0.04$ , which is considerably larger than measured from the light-curve solution ( $\sim 0.32$ ). Given that the spectroscopy and the light-curve fit produce consistent results for the flux ratios between each of the two stars in the 6 day binary and star Aa, the problem would appear to be with star Ab. Although in principle an error in our adopted temperature for that star could bias the spectroscopic light ratio (but is unlikely to affect the radial velocities), tests suggest that the required change in  $T_{\text{eff}}$  is much too large. Alternatively, we speculate that a bias in the spectroscopic light ratio could occur if star Ab were chemically peculiar (i.e., a metallic-line A star), in which case our synthetic templates would not be a good match to the real star. A-type stars with such anomalies are overwhelmingly members of binary systems and rotate more slowly than A stars in the field. The measured rotation rate of star Ab ( $\sim 40 \text{ km s}^{-1}$ ) is in fact slow enough to be in the range where these chemical anomalies are seen in other binaries. Confirmation of this hypothesis would require a detailed chemical analysis.

## 5. Comparison with Stellar Evolution Models

Eclipsing binaries with well-determined masses, radii, and temperatures provide some of strongest tests of stellar evolution theory available (Torres et al. 2010). The presence of four stars in V482 Per sharing a common age and chemical composition

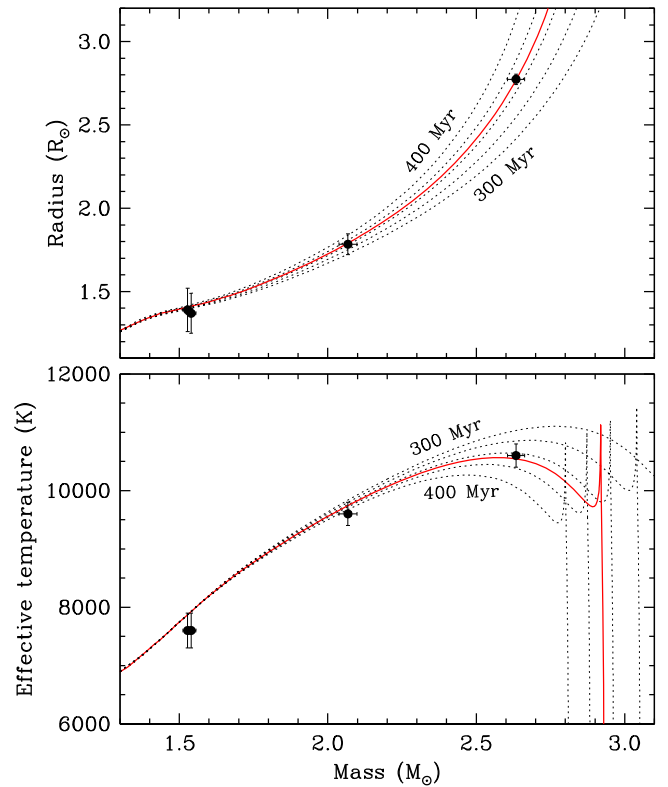


**Figure 10.** Measurements for V482 Per compared against model isochrones from the MIST series (Choi et al. 2016) for a metallicity of  $[\text{Fe}/\text{H}] = -0.15$  and ages of 300–400 Myr, in steps of 25 Myr. The best match is indicated by the solid curve, and corresponds to an age of 360 Myr.

offers an even stronger test. Figure 10 presents a comparison of the observations for V482 Per against model isochrones from the recent MESA Isochrones and Stellar Tracks (MIST) series by Choi et al. (2016), which is based on the Modules for Experiments in Stellar Astrophysics package (MESA; Paxton et al. 2011, 2013, 2015). The mass–radius diagram in the top panel indicates excellent agreement between theory and observation for a metallicity of  $[\text{Fe}/\text{H}] = -0.15$  and an age of 360 Myr constrained mostly by the properties of stars Aa and Ab. The slightly subsolar composition suggested by the models is close enough to the solar value adopted throughout our analysis that it has a negligible effect on our measurements of the system. The agreement with the stellar temperatures shown in the lower panel of the figure is also good for Aa and Ab; the Ba and Bb components appear only marginally cooler than predicted. The state of evolution of each star is seen more clearly in Figure 11, which shows evolutionary tracks from these models computed for the measured masses, along with the same best-fit isochrone as above. Stars Ba and Bb are near the zero-age main sequence, while Aa is more than halfway through its main-sequence lifetime.

Other models give similar results. For example, a comparison against isochrones from the Yonsei–Yale series (Yi et al. 2001; Demarque et al. 2004) yields a good match to the observations for an age of 375 Myr and a composition of  $[\text{Fe}/\text{H}] = -0.28$ . The difference in the best-fit compositions is simply a consequence of the adoption of different solar metallicities in these two series of models. MIST adopts the solar element mixture by Asplund et al. (2009), giving a metal content  $Z_{\odot} = 0.0134$ , whereas the Yonsei–Yale models adopt the mixture of Grevesse et al. (1996), in which  $Z_{\odot} = 0.0179$ .

<sup>9</sup> The conversion was performed using synthetic spectra by Husser et al. (2013) based on PHOENIX model atmospheres for the adopted temperatures of the components, and the radius ratios from Table 7.

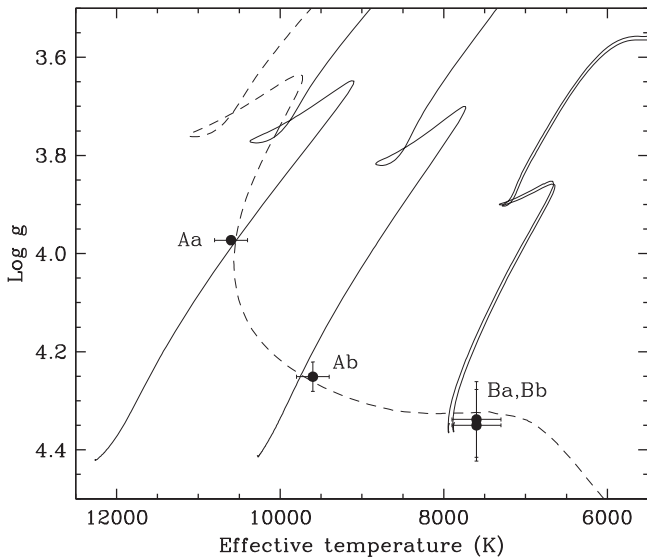


**Figure 11.** Evolutionary tracks from the MIST series (Choi et al. 2016) for the measured masses of the V482 Per components in the  $T_{\text{eff}}\text{-log } g$  plane. The dashed line represents the best-fit isochrone for an age of 360 Myr and  $[\text{Fe}/\text{H}] = -0.15$ .

The higher value for the latter models should then result in an  $[\text{Fe}/\text{H}]$  scale that is  $\log(0.0179/0.0134) \approx 0.13$  dex lower, which is precisely what we find. The small age difference between the two models is likely related to differences in their physical ingredients, such as the treatment of convective core overshooting and the helium abundance.

## 6. Discussion and Final Remarks

Binary stars and systems of higher multiplicity provide valuable insights into star formation and the role of dynamical and dissipative processes in shaping the architecture of stellar systems. Statistical studies indicate that hierarchical quadruple systems are relatively rare. Tokovinin (2014) reported a rate of occurrence among F- and G-type stars of only 4%, while De Rosa et al. (2014) found a smaller rate of about 2% among A stars. V482 Per is remarkable in that we are able to measure radial velocities of the four components and that both inner binaries display eclipses, yielding direct measurements of the masses and radii for all stars at a single age and composition. The first known example of such a doubly eclipsing quadruple system is BV Dra + BW Dra (Batten & Hardie 1965; Batten & Lu 1986), a wide visual pair with a  $16''$  angular separation that enables the two WUMa eclipsing binaries to be studied separately.

Several more doubly eclipsing quadruple systems that feature complex light curves have been found, but most have not yet been studied spectroscopically. Aside from V482 Per, we know of only four cases in which it has been possible to measure the radial velocities for all components from the quadruple-lined spectra to derive their physical properties: V994 Her (Lee et al. 2008; Zasche & Uhlir 2013, 2016), KIC 4247791 (Lehmann et al. 2012), 1SWASP J093010.78 +533859.5 (possibly a quintuple system; Koo et al. 2014; Lohr et al. 2015), and EPIC 220204960 (Rappaport et al. 2017). The outer orbit is known in only one of these cases (V994 Her) and in V482 Per. Additional examples of quadruple systems have been found in which one of the inner pairs eclipses, but not the other. A partial list includes LO Hya (with inner periods of

2.50 days and 5.97 days, which are remarkably similar to those in V482 Per; see Fekel 1981; Bakos 1985; Docobo & Ling 2007), V379 Cep (Harmanec et al. 2007), BD-22 5866 (Shkolnik et al. 2008), and KIC 7177553 (Lehmann et al. 2016).

The V482 Per system appears dynamically stable. To verify this we used the three-body hierarchical stability criterion of Eggleton & Kiseleva (1995), treating each binary as the perturbing third body for the other. The minimum period ratios for stability are  $P_{\text{outer}}/P_{\text{inner}} \sim 200$ , whereas the observed values are about 2500 for binary A and 1000 for binary B.

As reported in Section 3.2, one of the intriguing findings of the present investigation is the fairly large and apparently significant rate of *retrograde* apsidal precession in the slightly eccentric 6 day binary, in the amount of about  $60 \text{ deg century}^{-1}$ . Based on the measured stellar properties and theoretical internal structure constants ( $\log k_2$  of  $-2.41$  and  $-2.40$  for stars Ba and Bb, from Claret 2004), the rate of apsidal motion one would expect for the 6 day binary is  $2.62 \pm 0.16 \text{ deg century}^{-1}$  in the prograde sense, of which 82%, or  $2.15 \text{ deg century}^{-1}$ , is due to general relativity. Provided our measurement of  $\dot{\omega}_B$  is accurate, as discussed earlier, it would indicate that classical and relativistic effects are being overwhelmed by other forces that completely reverse the direction of net precession.

An effect that can act in such a way is a misalignment between the spin axes and the orbital axis of the binary. This was proposed by Shakura (1985) as an explanation for the anomalous apsidal motion rate measured for the eclipsing binary DI Her, which is four times slower than expected and had puzzled astronomers for decades. Albrecht et al. (2009) proved Shakura's idea to be correct by exploiting the Rossiter-McLaughlin effect and showing that the two stars rotate with their spin axes nearly perpendicular to the orbital axis, in such a way as to account for the observed discrepancy (see also Claret et al. 2010). Although a similar effect could be operating in the 6 day binary within V482 Per, it would not be sufficient to reverse the direction of the precession, particularly since the relativistic term dominates over the rotational terms.

An alternate possibility is dynamical interactions induced by the 2.4 day binary, especially given that the outer orbit is very eccentric ( $e = 0.8533$ ). At closest approach, the centers of mass of the two binaries come within 1.9 au of each other, or about 20 times the semimajor axis of the 6 day binary. At this distance, the 2.4 day binary may no longer appear to the other as a point source, but rather as a larger perturbing object the size of its own semimajor axis. Although it is not very common, normal prograde apsidal motion can be altered drastically and even reversed by the interactions (Eggleton & Kiseleva-Eggleton 2001; Borkovits et al. 2016), and will generally also lead to changes in other orbital elements, an effect we have not considered here. Examples of retrograde apsidal motion have been reported by, e.g., Borkovits et al. (2015), some as rapid as we see in V482 Per. Numerical simulations that are beyond the scope of this paper may be able to quantify the interactions more accurately, although our current knowledge of the quadruple system does not constrain the problem completely. For example, we do not know how the three orbits are oriented in space (relative inclinations), and hence their true directions of motion, which can have a significant impact on the perturbations. Only their line-of-sight inclinations have been measured. They happen to be quite similar to each other ( $i_A = 83.2 \pm 1.0^\circ$ ,  $i_B = 85.3 \pm 1.1^\circ$ , and

$i_{AB} = 79^{\circ}.6 \pm 6^{\circ}.4$ ), which might suggest near coplanarity. Studies of orbital alignment in hierarchical triple systems do in fact report that relatively tight triples with outer orbits having semimajor axes smaller than 50 au (V482 Per has 12.9 au; Table 7) tend to be aligned (Tokovinin 2017), although this appears to depend also on mass, with massive systems such as V482 Per being less aligned than low-mass systems, on average. If the three orbits in V482 Per are in fact closely aligned, this would be at odds with the known cases of retrograde apsidal motion in triple systems, which are found to occur in strongly misaligned or even counter-rotating configurations, driven by the Kozai–Lidov mechanism (e.g., Borkovits et al. 2011, 2015).

Measuring accurate times of eclipse for the 6 day binary would be highly beneficial to confirm or strengthen the determination of  $\dot{\omega}_B$ . Although the eclipses are shallow ( $\sim 2.3\%$ ), they are well within the detection limits of many observing facilities such as those used to search for transiting planets.

We are grateful to B. Beky, P. Berlind, Z. Berta, W. Brown, M. Calkins, G. Esquerdo, D. W. Latham, R. P. Stefanik, and G. Zhou for help in obtaining the spectroscopic observations of V482 Per, and to J. Mink for maintaining the CfA echelle database over the years. We thank J. Irwin for helpful discussions about the use of his light-curve code, T. Mazeh and M. Holman for conversations about the dynamics of multiple systems, and P. Harmanec for help in the initial stages of the analysis. The anonymous referee provided helpful comments on the original manuscript. The authors also wish to thank Dr. A. W. (Bill) Neely, who operated and maintained the NFO WebScope for the Consortium and who handled preliminary processing of the images and their distribution. The present analysis made use of Hydra, the Smithsonian Institution High Performance Cluster (SI/HPC). G.T. acknowledges partial support for this work from NSF grant AST-1509375. The research at Tennessee State University was made possible by NSF support through grant 1039522 of the Major Research Instrumentation Program. In addition, astronomy at Tennessee State University is supported by the state of Tennessee through its Centers of Excellence program. The research of M.W. was supported by grant GA15-02112S from the Czech Science Foundation. This work has made use of the SIMBAD and VizieR databases, operated at CDS, Strasbourg, France, and of NASA’s Astrophysics Data System Abstract Service.

### ORCID iDs

Guillermo Torres  <https://orcid.org/0000-0002-5286-0251>

Claud H. Sandberg Lacy  <https://orcid.org/0000-0002-0455-679X>

Francis C. Fekel  <https://orcid.org/0000-0002-9413-3896>

### References

- Agerer, F., Dahm, M., & Hübscher, J. 1999, *IBVS*, **4712**, 1
- Agerer, F., & Hübscher, J. 1995, *IBVS*, **4222**, 1
- Agerer, F., & Hübscher, J. 1996, *IBVS*, **4383**, 1
- Agerer, F., & Hübscher, J. 1997, *IBVS*, **4472**, 1
- Agerer, F., & Hübscher, J. 1998, *IBVS*, **4562**, 1
- Agerer, F., & Hübscher, J. 2003, *IBVS*, **5484**, 1
- Agerer, F., & Lichtenknecker, D. 1991, *IBVS*, **3554**, 1
- Albrecht, S., Reffert, S., Snellen, I. A. G., & Winn, J. N. 2009, *Natur*, **461**, 373
- Amôres, E. B., & Lépine, J. R. D. 2005, *AJ*, **130**, 659
- Andersen, J., Clausen, J. V., Nordstrom, B., Tomkin, J., & Mayor, M. 1991, *A&A*, **246**, 99
- Asplund, M., Grevesse, N., Sauval, A. J., & Scott, P. 2009, *ARA&A*, **47**, 481
- Bakos, G. A. 1985, *JRASC*, **79**, 119
- Baştürk, Ö, Zola, S., Liakos, A., et al. 2015, *NewA*, **41**, 42
- Batten, A. H., & Hardie, R. H. 1965, *AJ*, **70**, 666
- Batten, A. H., & Lu, W. 1986, *PASP*, **98**, 92
- Borkovits, T., Csizmadia, S., Forgács-Dajka, E., & Hegedüs, T. 2011, *A&A*, **528**, A53
- Borkovits, T., Hajdu, T., Sztakovics, J., et al. 2016, *MNRAS*, **455**, 4136
- Borkovits, T., Rappaport, S., Hajdu, T., & Sztakovics, J. 2015, *MNRAS*, **448**, 946
- Brát, L., Zejda, M., & Svoboda, P. 2007, *OEJV*, **74**, 1
- Brooks, S. P., & Gelman, A. 1997, *J. of Computational and Graphical Statistics*, **7**, 434
- Choi, J., Dotter, A., Conroy, C., et al. 2016, *ApJ*, **823**, 102
- Claret, A. 2004, *A&A*, **424**, 919
- Claret, A., & Bloemen, S. 2011, *A&A*, **529**, A75
- Claret, A., Torres, G., & Wolf, M. 2010, *A&A*, **515**, A4
- Demarque, P., Woo, J.-H., Kim, Y.-C., & Yi, S. K. 2004, *ApJS*, **155**, 667
- De Rosa, R. J., Patience, J., Wilson, P. A., et al. 2014, *MNRAS*, **437**, 1216
- Diethelm, R. 2009, *IBVS*, **5894**, 1
- Diethelm, R. 2011a, *IBVS*, **5960**, 1
- Diethelm, R. 2011b, *IBVS*, **5992**, 1
- Diethelm, R. 2013, *IBVS*, **6042**, 1
- Docobo, J. A., & Ling, J. F. 2007, *AJ*, **133**, 1209
- Drimmel, R., Cabrera-Lavers, A., & López-Corredoira, M. 2003, *A&A*, **409**, 205
- Eaton, J. A., & Williamson, M. H. 2007, *PASP*, **119**, 886
- Eggleton, P., & Kiseleva, L. 1995, *ApJ*, **455**, 640
- Eggleton, P. P., & Kiseleva-Eggleton, L. 2001, *ApJ*, **562**, 1012
- Etzel, P. B. 1981, in *Photometric and Spectroscopic Binary Systems*, ed. E. B. Carling & Z. Kopal (Dordrecht: Reidel), **111**
- Fekel, F. C., Rajabi, S., Muterspaugh, M. W., & Williamson, M. H. 2013, *AJ*, **145**, 111
- Fekel, F. C., Tomkin, J., & Williamson, M. H. 2009, *AJ*, **137**, 3900
- Fekel, F. C., Jr. 1981, *ApJ*, **246**, 879
- Flower, P. J. 1996, *ApJ*, **469**, 355
- Foreman-Mackey, D. 2016, *JOSS*, **1**, 24
- Foreman-Mackey, D., Hogg, D. W., Lang, D., & Goodman, J. 2013, *PASP*, **125**, 306
- Fűrész, G. 2008, PhD thesis, Univ. Szeged
- Gelman, A., & Rubin, D. B. 1992, *StatSci*, **7**, 457
- Goodman, J., & Weare, J. 2010, *Commun. Appl. Math. Comput. Sci.*, **5**, 65
- Grauer, A. D., Neely, A. W., & Sandberg Lacy, C. H. 2008, *PASP*, **120**, 992
- Gray, D. F. 1992, *The Observation and Analysis of Stellar Photospheres*, Vol. 20 (2nd ed.; New York: Wiley), **430**
- Green, G. M., Schlafly, E. F., Finkbeiner, D. P., et al. 2015, *ApJ*, **810**, 25
- Grevesse, N., Noels, A., & Sauval, A. J. 1996, in *ASP Conf. Ser. 99, Cosmic Abundances*, ed. S. S. Holt & G. Sonneborn (San Francisco, CA: ASP), **117**
- Hakkila, J., Myers, J. M., Stidham, B. J., & Hartmann, D. H. 1997, *AJ*, **114**, 2043
- Harmanec, P., Mayer, P., Prša, A., et al. 2007, *A&A*, **463**, 1061
- Harvig, V., & Leis, L. 1981, *PTarO*, **48**, 172
- Heckmann, O. 1975, in *AGK 3. Star Catalogue of Positions and Proper Motions North of  $-2.5$  deg. Declination*, ed. W. Dieckvoss (Hamburg-Bergedorf: Hamburger Sternwarte)
- Hoffmeister, C. 1966, *AN*, **289**, 1
- Hübscher, J., Agerer, F., Frank, P., & Wunder, E. 1994, *BAV Mitteilungen*, **68**, 7
- Hübscher, J., Agerer, F., & Wunder, E. 1991, *BAV Mitteilungen*, **59**, 7
- Hübscher, J., Agerer, F., & Wunder, E. 1992, *BAV Mitteilungen*, **60**, 7
- Hübscher, J., Agerer, F., & Wunder, E. 1993, *BAV Mitteilungen*, **62**, 6
- Hübscher, J., & Lehmann, P. B. 2015, *IBVS*, **6149**, 1
- Hübscher, J., Lehmann, P. B., & Walter, F. 2012, *IBVS*, **6010**, 1
- Hübscher, J., Steinbach, H.-M., & Walter, F. 2009a, *IBVS*, **5874**, 1
- Hübscher, J., Steinbach, H.-M., & Walter, F. 2009b, *IBVS*, **5889**, 1
- Hübscher, J., & Walter, F. 2007, *IBVS*, **5761**, 1
- Husser, T.-O., Wende-von Berg, S., Dreizler, S., et al. 2013, *A&A*, **553**, A6
- Hut, P. 1981, *A&A*, **99**, 126
- Irwin, J. B. 1952, *ApJ*, **116**, 211
- Irwin, J. B. 1959, *AJ*, **64**, 149
- Irwin, J. M., Quinn, S. N., Berta, Z. K., et al. 2011, *ApJ*, **742**, 123
- Juryšek, J., Hoňková, K., Šmelcer, L., et al. 2017, *OEJV*, **179**, 1
- Koo, J.-R., Lee, J. W., Lee, B.-C., et al. 2014, *AJ*, **147**, 104
- Kotková, L., & Wolf, M. 2006, *IBVS*, **5676**, 1

- Lacy, C. H. S. 2002, *IBVS*, **5357**, 1
- Lacy, C. H. S. 2003, *IBVS*, **5487**, 1
- Lacy, C. H. S. 2004, *IBVS*, **5577**, 1
- Lacy, C. H. S. 2006, *IBVS*, **5670**, 1
- Lacy, C. H. S. 2007, *IBVS*, **5764**, 1
- Lacy, C. H. S. 2009, *IBVS*, **5910**, 1
- Lacy, C. H. S. 2011, *IBVS*, **5972**, 1
- Lacy, C. H. S. 2012, *IBVS*, **6014**, 1
- Lacy, C. H. S. 2013, *IBVS*, **6046**, 1
- Lacy, C. H. S., & Fekel, F. C. 2011, *AJ*, **142**, 185
- Lacy, C. H. S., Torres, G., & Claret, A. 2008, *AJ*, **135**, 1757
- Lacy, C. H. S., Torres, G., Claret, A., & Vaz, L. P. R. 2005, *AJ*, **130**, 2838
- Lee, C.-U., Kim, S.-L., Lee, J. W., et al. 2008, *MNRAS*, **389**, 1630
- Lehmann, H., Borkovits, T., Rappaport, S. A., et al. 2016, *ApJ*, **819**, 33
- Lehmann, H., Zechmeister, M., Dreizler, S., Schuh, S., & Kanzler, R. 2012, *A&A*, **541**, A105
- Liakos, A., & Niarchos, P. 2011, *IBVS*, **6005**, 1
- Lindgren, L., Lammers, U., Bastian, U., et al. 2016, *A&A*, **595**, A4
- Lohr, M. E., Norton, A. J., Gillen, E., et al. 2015, *A&A*, **578**, A103
- Luo, A. L., Zhao, Y.-H., Zhao, G., et al. 2016, *VizieR Online Data Catalog: LAMOST DR2 catalogs*
- Ogloza, W., Kreiner, J. M., Stachowski, G., et al. 2012, in *IAU Symp. 282, From Interacting Binaries to Exoplanets: Essential Modeling Tools*, ed. M. T. Richards & I. Hubeny (Cambridge: Cambridge Univ. Press), **85**
- Paschke, A. 2017, *O-C Gateway, Variable Star and Exoplanet Section*, <http://var2.astro.cz/ocgate/ocgate.php?star=V0482+Per&lang=en>
- Pawlak, M., Graczyk, D., Soszyński, I., et al. 2013, *AcA*, **63**, 323
- Paxton, B., Bildsten, L., Dotter, A., et al. 2011, *ApJS*, **192**, 3
- Paxton, B., Cantiello, M., Arras, P., et al. 2013, *ApJS*, **208**, 4
- Paxton, B., Marchant, P., Schwab, J., et al. 2015, *ApJS*, **220**, 15
- Pickles, A., & Depagne, É. 2010, *PASP*, **122**, 1437
- Popper, D. M. 1980, *ARA&A*, **18**, 115
- Popper, D. M. 1996, *ApJS*, **106**, 133
- Popper, D. M., & Etzel, P. B. 1981, *AJ*, **86**, 102
- Prša, A., Harmanec, P., Torres, G., et al. 2016, *AJ*, **152**, 41
- Rappaport, S., Vanderburg, A., Borkovits, T., et al. 2017, *MNRAS*, **467**, 2160
- Scarfè, C. D. 2010, *Obs*, **130**, 214
- Schlegel, D. J., Finkbeiner, D. P., & Davis, M. 1998, *ApJ*, **500**, 525
- Shakura, N. I. 1985, *SvAL*, **11**, 224
- Shkolnik, E., Liu, M. C., Reid, I. N., et al. 2008, *ApJ*, **682**, 1248
- Szentgyorgyi, A. H., & Fűrész, G. 2007, in *Rev. Mex. Astron. Astrof. Conf. Ser. 28, Telescopes of the Future and San Pedro Martir*, ed. S. Kurtz et al. (Mexico City: UNAM), 129
- Tokovinin, A. 2014, *AJ*, **147**, 87
- Tokovinin, A. 2017, *ApJ*, **844**, 103
- Torres, G. 2010, *AJ*, **140**, 1158
- Torres, G., Andersen, J., & Giménez, A. 2010, *A&ARv*, **18**, 67
- Torres, G., Latham, D. W., & Stefanik, R. P. 2007, *ApJ*, **662**, 602
- Torres, G., McGruder, C. D., Siverd, R. J., et al. 2017, *ApJ*, **836**, 177
- Torres, G., Neuhäuser, R., & Guenther, E. W. 2002, *AJ*, **123**, 1701
- Wolf, M., Mayer, P., Zasche, P., Sarounova, L., & Zejda, M. 2004, in *ASP Conf. Ser. 318, Spectroscopically and Spatially Resolving the Components of Close Binary Stars*, ed. R. W. Hilditch, H. Hensberge, & K. Pavlovski (San Francisco, CA: ASP), **255**
- Yi, S., Demarque, P., Kin, Y.-C., et al. 2001, *ApJS*, **136**, 417
- Yilmaz, M., Basturk, O., Alan, N., et al. 2009, *IBVS*, **5887**, 1
- Zacharias, N., Finch, C., Subasavage, J., et al. 2015, *AJ*, **150**, 101
- Zasche, P., & Uhlař, R. 2013, *MNRAS*, **429**, 3472
- Zasche, P., & Uhlař, R. 2016, *A&A*, **588**, A121
- Zasche, P., Uhlař, R., Svoboda, P., et al. 2017, *IBVS*, **6204**, 1
- Zejda, M. 2004, *IBVS*, **5583**, 1
- Zucker, S., & Mazeh, T. 1994, *ApJ*, **420**, 806